COMPARATIVE ANALYSIS OF FMVSS 208 SLED AND DYNAMIC DECELERATION PULSE CHARACTERISTICS

Jai Singh
Biomechanical Engineering Analysis & Research, Inc.
United States

John Perry
Autodyne, Inc.
United States
Paper Number 05-0028

ABSTRACT

Equivalent half sine approximations derived from accelerometer data for Federal Motor Vehicle Safety Standard (FMVSS) 208 dynamic compliance testing and other substantially similar non-FMVSS, non-New Car Assessment Program (NCAP) tests were characterized in terms of amplitude, circular frequency, time duration and displacement. The results were compared and contrasted with the idealized and actualized FMVSS 208 sled deceleration pulses. A total of 346 dynamic tests and 83 sled tests were considered. For the passenger vehicle subset of the FMVSS 208 dynamic test population these parameters were 224.98 ± 30.39 m/sec^2, 34.11 ± 4.57 sec^{-1}, 94 ± 13 msec and 0.619 ± 0.089 meters respectively. For the multipurpose vehicle subset of the FMVSS 208 dynamic test population theses parameters were 246.17 ± 43.61 m/sec^2, 37.78 ± 6.38 sec^{-1}, 86 ± 15 msec and 0.557 ± 0.100 meters respectively. The differences in all parameters between the two classifications were significant ($p < 0.00004$). For the dynamic frontal impact population *en toto* the valuations of these parameters for the passenger vehicle classification were 225.10 ± 29.07 m/sec^2, 34.26 ± 4.26 sec^{-1}, 93 ± 12 msec and 0.612 ± 0.085 meters respectively whereas for the multipurpose vehicle classification they were 243.82 ± 43.37 m/sec^2, 37.50 ± 6.28 sec^{-1}, 86 ± 15 msec and 0.560 ± 0.102 meters respectively. The differences in all parameters between the two classifications were significant ($p < 0.0001$). The corresponding parameters for the target half sine deceleration pulse of the FMVSS 208 sled test are 168.73 m/sec^2, 25.12 sec^{-1}, 125 msec and 0.839 meters. The sled half sine deceleration pulse substantially underestimates the characteristic mean response obtained from the half sine equivalents of dynamic tests.

INTRODUCTION

The full-width engagement perpendicular impact of a vehicle under consideration into a fixed, rigid, massive barrier has long served as a means of assessing frontal impact protection. This form of testing, in the United States, has been codified in the form of Federal Motor Vehicle Safety Standard (FMVSS) 208. Prior to the consideration and implementation of other testing configurations under this standard, the FMVSS 208 compliance test consisted of a 48 KPH (30 MPH) closing speed impact of an instrumented test vehicle under the above-described conditions. With the ubiquitous use of supplemental restraint systems (SRS) in the vehicle fleet, the issue of air bag aggressivity has arisen as a potential cause of serious or lethal injury to certain segments of the general populace. The underlying necessity for rapid testing of alternative (depowered) frontal air bag systems has served as a basis for the implementation of an alternative compliance procedure. This alternative procedure consists of a non-impact test in which the vehicle under consideration is rigidly mounted to a sled and the sled is subjected to the half sine pulse described by equation (1) in which deceleration is in units of m/sec^2.

$$\ddot{x}(t) = -168.73 \cdot Sin\left(\frac{\pi \cdot t}{0.125}\right) \qquad (1).$$

The sled and the test vehicle, as a consequence of rigid coupling, experience the deceleration shown by equation (1). Explicit integration of equation (1) over the pulse duration results in a solution for the change in speed incurred of -13.427 m/sec (30.04 MPH). Implicit integration of equation (1), followed by the application of the initial condition of $\dot{x}(0) = 0$ followed by explicit integration over the pulse duration results in a solution for the displacement over which the pulse is applied. This displacement is -0.839 meters (33.0 inches).

The sled pulse is bounded, as per stated requirement, by both a maximum and a minimum corridor. The maximum corridor is defined by a linear change in acceleration from 0 G at 5 msec to -16 G at 55 msec, a plateau at -16 from 55 msec to 70

msec and a linear change to 0 G at 120 msec. The minimum corridor is defined by a linear change in acceleration from -2 G at 0 msec to -18.2G at 40 msec, a plateau at -18.2 G from 40 msec to 85 msec and a linear change to 0G at 130 msec. The maximum and minimum acceleration corridors are ideal in nature, which if matched exactly would result in change in speed of -10.23 m/sec (-22.83 MPH) and -16.08 m/sec -(35.96 MPH) respectively. In that these corridors are ideal and that the actual pulse is half sine in form, one may utilize the former to determine the characteristics of the closest approximating ideal half sine pulses with the same respective impact durations and onset/end times. These curves, for the maximum and minimum corridor, provide changes in speed of -11.737 m/sec (-26.255 MPH) and -14.660 m/sec (-32.793 MPH) respectively. The derivation of these results is shown in Appendix A and the results are shown in Figure 1.

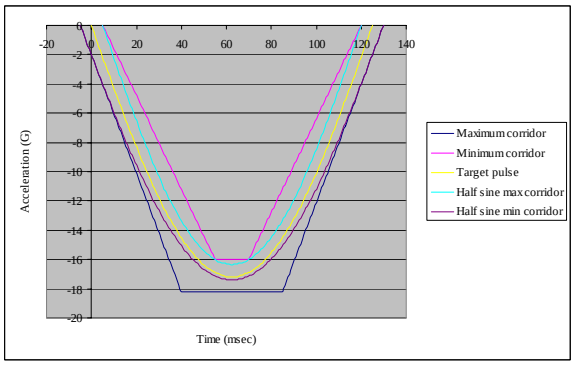

Figure 1. Acceleration corridors, target half sine pulse and admissible half sine pulses for the FMVSS 208 sled test.

Lumped Mass Model

Lumped parameter (LP) models have been utilized for a number of years in evaluating the collision response of motor vehicles. The simplest of these models treats the total vehicle mass as a single lumped parameter. The vehicle frontal structures are modeled as a single uniaxial linear spring characterized by a spring constant *k*. The half sine collision pulse is the characteristic response of the single lumped mass linear spring uniaxial model subjected to dissipative function *F* with particular solution *C*t where *C* is a constant. This dissipative function is necessary for removal of the oscillatory nature of motion associated with the LP model. Furthermore, it allows for kinematic modeling of the collision pulse over half of the full sine wave period. For full-width engagement front to rigid, fixed, massive barrier impacts, the system is subject to the initial conditions of $\dot{x}(t=0)=v_0$ and $x(t=0)=0$. This model is shown in Figure 2.

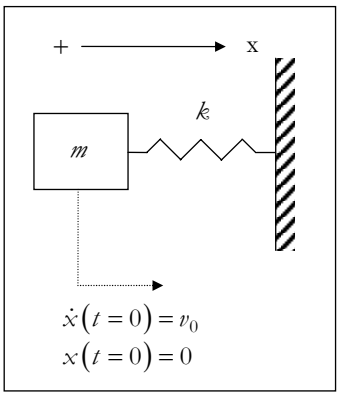

Figure 2. SDOF lumped mass and linear spring model of the FMVSS 208 compliance test.

The equation of motion for this system is given by the following second order differential equation.

$$m\ddot{x}(t)+kx(t)=F \qquad (2).$$

The solutions for the system displacement, velocity and acceleration, as derived in Appendix B, are given by equations (3-5) respectively.

$$x(t)=\frac{v_o\cdot T_{impact}}{2\cdot\pi}\cdot Sin\left(\frac{\pi\cdot t}{T_{impact}}\right)+\frac{v_o}{2}\cdot t \qquad (3).$$

$$\dot{x}(t)=\frac{v_o}{2}\cdot Cos\left(\frac{\pi\cdot t}{T_{impact}}\right)+\frac{v_o}{2} \qquad (4).$$

$$\ddot{x}(t)=-\frac{v_o\cdot\pi}{2\cdot T_{impact}}\cdot Sin\left(\frac{\pi\cdot t}{T_{impact}}\right) \qquad (5).$$

The solution for the homogeneous part of equation (3) can be substituted into the corresponding unforced response of equation (2) in order to solve for the circular frequency in terms of the system parameters *m* and *k*.

$$\omega_n=\sqrt{\frac{k}{m}} \qquad (6).$$

Equation (5) can be rewritten by noting that the peak acceleration occurs when the sine function obtains a value of unity resulting in a solution of $A_p=-0.5\cdot v_0\cdot\omega_n$.

$$\ddot{x}(t) = A_p \cdot \sin(\omega_n \cdot t) \qquad (7).$$

Collision Pulse Modeling

Huang [2002] proposed a method for deriving the solution for the amplitude and the circular frequency for the equivalent half sine pulse for a given acceleration-time history obtained from a vehicle fixed accelerometer. Implicit in this formulation is the consistency between the vehicle fixed accelerometer time history and the dynamic center of mass deceleration. Integrating equation (7) implicitly results in the solution for the velocity-time history.

$$\dot{x}(t) = \int \ddot{x}(t)\,dt = -\frac{A_p}{\omega_n} \cdot \cos(\omega_n \cdot t) + c_1 \qquad (8).$$

Again, the velocity solution is subject to the initial condition of $\dot{x}(t=0) = v_0$ resulting in the following solution for c_1.

$$\dot{x}(0) = v_0 = -\frac{A_p}{\omega_n} + c_1 \rightarrow c_1 = v_0 + \frac{A_p}{\omega_n} \qquad (9).$$

The velocity solution, obtained following the substitution of equation (9) into equation (8) is shown by equation (10).

$$\dot{x}(t) = -\frac{A_p}{\omega_n} \cdot \cos(\omega_n \cdot t) + \left(v_0 + \frac{A_p}{\omega_n}\right) \qquad (10).$$

The implicit integration of equation (10) results in displacement solution given in equation (11).

$$x(t) = \int \dot{x}(t)\,dt = -\frac{A_p}{\omega_n^2} \cdot \sin(\omega_n \cdot t) + \left(v_0 + \frac{A_p}{\omega_n}\right) \cdot t + c_2 \qquad (11).$$

The constant of integration c_2 can be shown to be equal to zero by imposition of the initial condition of zero displacement at time t = 0. Imposition of the boundary condition of zero velocity at the time of maximum displacement, t_m, results in the following form of equation (10).

$$\dot{x}(t_m) = 0 = -\frac{A_p}{\omega_n} \cdot \cos(\omega_n \cdot t) + \left(v_0 + \frac{A_p}{\omega_n}\right) \qquad (12).$$

The amplitude is thus:

$$A_p = \frac{-v_0 \cdot \omega_n}{1 - Cos(\omega_n \cdot t_m)} \qquad (13).$$

Imposition of the displacement boundary condition at time $t = t_m$ results in the solution for the circular frequency.

$$x(t_m) = A_p \cdot \left(\frac{t_m}{\omega_n} - \frac{1}{\omega_n^2} \cdot Sin(\omega_n \cdot t_m)\right) + (v_0 \cdot t_m) \qquad (14).$$

Substitution of equation (13) into equation (14) results in the following solution:

$$\frac{x(t_m)}{v_0 \cdot t_m} = 1 - \frac{\omega_n \cdot t_m - Sin(\omega_n \cdot t_m)}{(\omega_n \cdot t_m) \cdot (1 - Cos(\omega_n \cdot t_m))} \qquad (15).$$

Equation (15) can be solved numerically for ω_n and the result can then be substituted into equation (13) to solve for the peak acceleration A_p.

An alternative procedure, which avoids the use of an iterative solution for the circular frequency, follows that proposed by Varat and Husher [2003]. The subject implementation of this formulation reduces to one in which the only system unknown was the impact duration T_{impact}. Equation (7) can be integrated following substitution of the definition of the amplitude in terms of the circular frequency and initial velocity and the initial condition of the speed at impact at time t = 0 can be substituted in order to solve for the constant of integration.

$$\dot{x}(t) = -\frac{T_{impact} \cdot A_p}{\pi} \cdot Cos\left(\frac{\pi \cdot t}{T_{impact}}\right) + \left(v_0 + \frac{T_{impact} \cdot A_p}{\pi}\right) \qquad (16).$$

Integration of equation (16) followed by the application of the initial condition of $x(t=0) = 0$ results in the solution for the displacement.

$$x(t) = -\frac{T_{impact}^{\,2} \cdot A_p}{\pi^2} \cdot Sin\left(\frac{\pi \cdot t}{T_{impact}}\right) + t \cdot \left(v_0 + \frac{T_{impact} \cdot A_p}{\pi}\right) \qquad (17).$$

Implementation of the boundary condition of $\dot{x}(t = T_{impact}) = 0$ allows for the development of a solution for the amplitude in terms of the initial velocity and the impact duration.

$$A_p = -\frac{v_0 \cdot \pi}{2 \cdot T_{impact}} \quad (18).$$

Varat and Husher [2003] utilized the velocity boundary condition of $\dot{x}\left(t = T_{mipact}\right) = v_0 + \Delta v$ in deriving their kinematic relationships.

In the subject investigation, in order to match the previously derived pulse modeling and LP modeling work, the boundary condition of the occurrence of peak deflection at the time of zero velocity following impact was utilized. Substitution of this boundary condition, $x\left(t = T_{impact}\right) = x_{\max}$ and equation (18) into equation (17) results in the following solution for the impact duration in terms of the maximum displacement and initial velocity.

$$T_{impact} = \frac{2 \cdot x_{\max}}{v_0} \quad (19).$$

Equation (19) can be solved for given the maximum displacement from doubly integrated vehicle fixed accelerometer data and the *a priori* known velocity. The results can then be substituted into equation (7), equation (16) and equation (17) to solve for the acceleration, velocity and displacement time history for the half sine model.

$$\ddot{x}(t) = -\frac{v_0 \cdot \pi}{2 \cdot T_{impact}} \cdot \sin\left(\frac{\pi \cdot t}{T_{impact}}\right) \quad (20).$$

$$\dot{x}(t) = \frac{v_0}{2} \cdot Cos\left(\frac{\pi \cdot t}{T_{impact}}\right) + \left(\frac{v_0}{2}\right) \quad (21).$$

$$x(t) = \frac{T_{impact} \cdot v_0}{2 \cdot \pi} \cdot Sin\left(\frac{\pi \cdot t}{T_{impact}}\right) + t \cdot \left(\frac{v_0}{2}\right) \quad (22).$$

This formulation for the half sine model allows for the exact matching of the test vehicle change in speed (from the initial impact velocity to zero) and peak displacement solutions between the half sine pulse model and the single degree of freedom LP model.

Existing Concerns Regarding the 208 Sled Test

A number of concerns have been raised in regards to the use of the FMVSS 208 sled protocol in lieu of the full-scale barrier impact test [Hollowell et al., 1999]. These concerns include but are not limited to the inability, by means of sled testing, of evaluating vehicle frontal structural collision performance, the evaluation of occupant frontal crash protection, the evaluation of the actual timing of the frontal crash supplemental restraint systems and the inability to asses injury modalities associated with vehicle intrusion. In the context of kinematic constraints, differences exist between the FMVSS 208 dynamic and sled test protocols. In the former, the impact speed is fixed as being 48.0 ± 0.8 KPH (29.8 ± 0.5 MPH). The manner in which a particular test vehicle absorbs the kinetic energy associated with this barrier impact speed (i.e. deceleration characteristics) is dependent on the structure of the test vehicle. The sled test, conversely, provides for a fixed non-impact deceleration pulse that produces a change in speed of 48.3 KPH (30.04 MPH) under ideal implementation. Therefore, in both cases, discounting restitution for the barrier impact, the test vehicle undergoes a change in speed of approximately 48 KPH but the manner in which that change in speed occurs is markedly different.

OBJECTIVES

The primary objective of the subject study was to perform a population based analysis on the publicly accessible FMVSS 208 dynamic and equivalent research dataset for model years 1990 through 2005 in the context of quantifying the equivalent half sine acceleration pulse parameters and comparing the results to the FMVSS 208 sled test implementation.

METHODS

The NHTSA Vehicle Crash Test Database (VCTB) was queried for FMVSS 208 dynamic, FMVSS 208 sled and research tests matching the FMVSS 208 dynamic impact configuration and impact speed. Data was obtained for tests from fiscal years 1990 through 2005. For dynamic tests, the year range of 1990 through 1998 was utilized for consistency with previous studies [Hollowell et al., 1998; Hollowell et al., 1999]. Data from FMVSS 208 dynamic testing for fiscal years 1999 through 2005 was also considered in order to provide for the most current data and to evaluate the temporal effect, if any, regarding the introduction of the alternative test procedure on the equivalent half sine acceleration pulse parameters. Full-scale perpendicular front to rigid or load-cell equipped barrier impacts were also considered. The set of tests for this category was limited to those in which the barrier impact speed

was consistent with the FMVSS 208 dynamic requirements. For each dynamic collision test, UDS-1992 formatted data was imported into NHTSA's Plot Browser software program. Accelerometer data from the longitudinal (X) axis of a vehicle fixed accelerometer was filtered using a 60 Hz low-pass filter as per Society of Automotive Engineers (SAE) J211 standard. Filtered accelerometer data was then exported in {time, acceleration} format into a text file and then imported into a symbolic mathematics program [Mathematica v 5.0; Wolfram Research, Champaign, Illinois, USA]. Maximum deflection was determined from the double time integration of the accelerometer data. The half sine acceleration pulse parameters were determined using the relationships described previously. Tests in which the velocity-time history exhibited positive valued velocities following separation from the barrier face were excluded from the subject study. Also, tests in which the Newton-Raphson iterative method failed to converge for the solution to the circular frequency utilizing Huang's [2002] method were excluded.

Sled deceleration data was obtained in the same manner as for the dynamic tests. X-axis acceleration data was filtered using a 60 Hz low-pass filter and compared against the idealized half sine pulse and maximum/minimum trapezoidal corridors for consistency.

All statistical testing was conducted using either the Analyze-It [v. 1.72; Analyze-It Software, Ltd; Leeds, UK] add-in for Excel [Microsoft Corporation; Redmond, Washington, USA] or with the S-Plus [v. 6.0; Insightful Corporation; Seattle, Washington, USA]. Certain charts were generated using SigmaPlot [v. 7.101; SPSS; Chicago, Illinois, USA].

RESULTS

Dataset Characterization

A total of 447 tests were considered. Of these tests a total of 364 tests were dynamic and 83 were sled tests. Of the total number of dynamic tests, 265 tests were conducted under FMVSS 208 contract and 99 tests were under research contract. A total of six FMVSS 208 dynamic and 12 research tests were excluded in accordance with the criteria stated in the *Methods* section. The total number of dynamic tests considered was thus 346.

An evaluation of the total number of tests conducted under FMVSS 208 contract revealed an average of 31 tests conducted between fiscal years 1990 through 1997 with a drop noted for fiscal years 1996 and 1997. This can be contrasted to the average number of tests per fiscal year between 1998 and 2005 of 13 tests. This latter figure, however, may be more indicative, particularly for fiscal years from 2003 through 2005, of availability of test data from the VCTB rather than the total tests actually conducted. The total number of FMVSS 208 tests conducted per fiscal year and the distribution of these tests between the dynamic and sled protocols is shown in Figure 3.

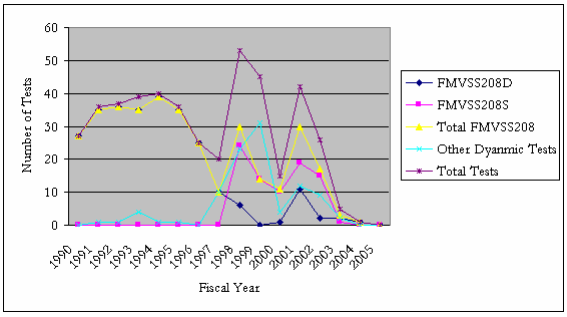

Figure 3. Total number of FMVSS 208 tests conducted on a fiscal year basis. Dynamic tests are limited to those that were involved in perpendicular impacts with rigid barriers. The first fiscal year during which the alternative sled test protocol was utilized was 1998. The data is discrete but is shown connected in a piecewise linear fashion for ease of visualization.

The total number of sled tests exceeded the total number of dynamic tests, per fiscal year, for every year following the introduction of the optional sled test protocol except for fiscal years 2003 and 2004. Over the same range of fiscal years (i.e. 1990 through 1997 contrasted to 1998 through 2005) the yearly average of the number of research tests meeting the criterion set forth in the *Methods* was 2 and 10 respectively.

The total number of FMVSS 208 dynamic tests involving passenger vehicles varied between 17 (FY 1996) and 35 (FY 1991) with a large drop noted for all fiscal years following 1996. The total number of research tests involving passenger vehicles remained relatively low ($N \leq 6$) for fiscal years prior to and including 1996, increased over the years of 1997 through 1999 and returned to a relatively low count for subsequent years. The total number of FMVSS dynamic tests involving multiple purpose vehicles (MPVs) peaked in 1992 with 16 vehicles tested, retained a relatively constant value of 8 or 9 vehicles per fiscal year between 1993 and 1996 and dropped for all subsequent years. The total number of other dynamic tests involving MPVs followed the general

trend observed for passenger vehicles with the number of vehicles increasing from 3 vehicles for fiscal year 1997 to 8 vehicles for fiscal years 1998 and peaking at 12 vehicles for fiscal year 1999. The number of MPVs tested for subsequent years was variable. These results are shown graphically in Figure 4.

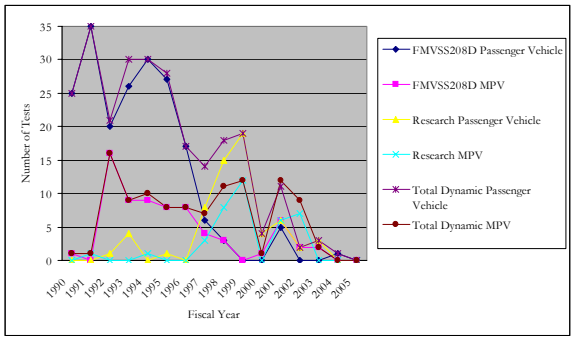

Figure 4. Distribution of dynamic tests by type (FMVSS 208 v. other) and by vehicle type (PV v. MPV).

Pulse Modeling

The method proposed by Huang [2002] did not ubiquitously provide estimates for the half sine amplitude and circular frequency that allowed for the correct reconstruction of the *a priori* barrier impact speed and displacement. As an example of the differences in the resultant equivalent half sine models produced, consider NHTSA test number v2463. This test was the FMVSS 208 dynamic compliance test for the 1997 Chrysler Sebring Convertible. The impact speed, time of peak displacement and value of peak displacement were 13.11 m/sec, 74.16 msec and 0.611 meters respectively. Numerically solving equation (15) and using the result to solve equation (13) resulted in a solution of -262.63 m/sec^2 for the equivalent half sine acceleration pulse amplitude and 23.60 sec^{-1} for the equivalent half sine acceleration pulse circular frequency. Conversely, use of equations (19), (18) and the relationship between the amplitude, circular frequency and initial velocity resulted in a solution of -220.96 m/sec^2 for the equivalent half sine acceleration pulse amplitude and 33.70 sec^{-1} for the equivalent half sine acceleration pulse circular frequency. The equivalent half sine waves, overlayed upon the filtered test data, are shown in Figure 5.

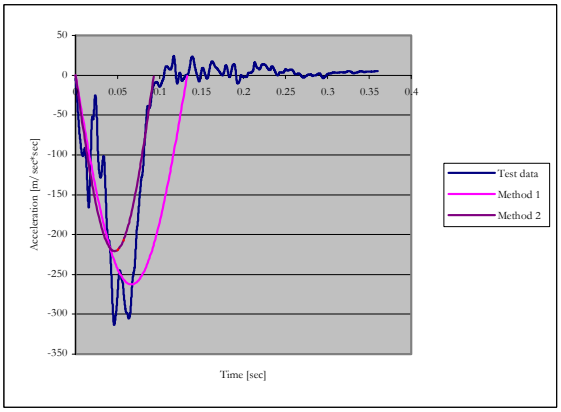

Figure 5. Equivalent half sine acceleration approximations generated by use Huang's method (Method 1) and the modified Varat and Husher method (Method 2) overlayed upon the test data from NHTSA test number v2463.

Determination of the change in speed incurred by the test vehicle by integration of each of the equivalent half sine acceleration pulses over the pulse duration resulted in a solution of -22.26 m/sec for Huang's method and 13.11 m/sec for the modified Varat and Husher method. The displacement during the pulse was calculated as being -1.482 meters and -0.611 meters for each method respectively.

FMVSS 208 Dynamic Tests

The mean and standard deviation of the peak deflection from the double integrated vehicle fixed accelerometer data, equivalent half sine acceleration pulse amplitude, equivalent half sine acceleration pulse circular frequency and equivalent half sine acceleration pulse duration were determined per fiscal year for the FMVSS 208 dynamic tests following categorization of individual tests into the appropriate vehicle class (passenger vehicle vs. multi purpose vehicle). The results are shown in Figures 6-9. Mean values are shown as the top of the corresponding bar for each vehicle class for each fiscal year for which test data was available. Standard deviations are shown as error bars positioned above the mean values. Mean valuations for which no error bars are shown represent data obtained from single tests. Fiscal years for which no mean value is shown indicate the lack of corresponding test data.

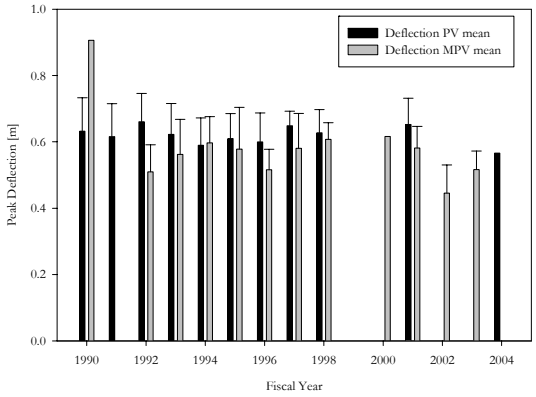

Figure 6. Means and standard deviations of peak deflections per fiscal year for FMVSS 208 dynamic tests.

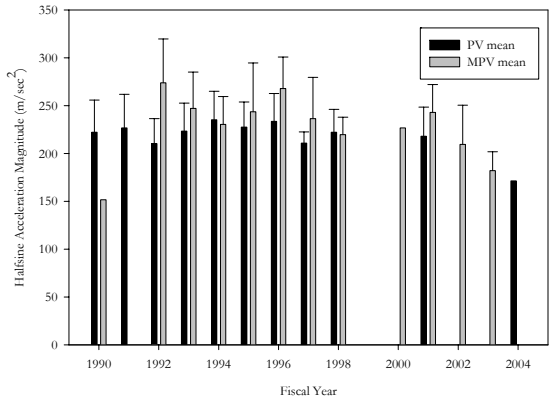

Figure 7. Mean and standard deviations of half sine amplitudes per fiscal year for FMVSS 208 dynamic tests.

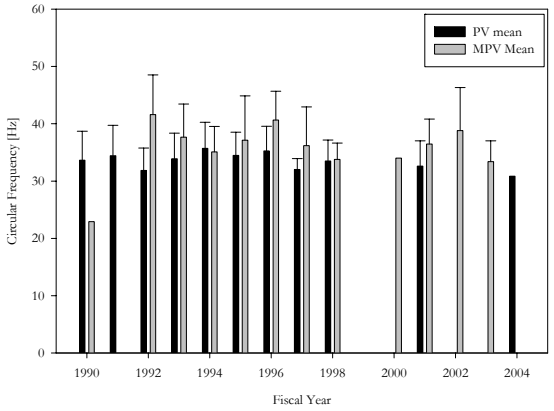

Figure 8. Mean and standard deviations of half sine circular frequencies per fiscal year for FMVSS 208 dynamic tests.

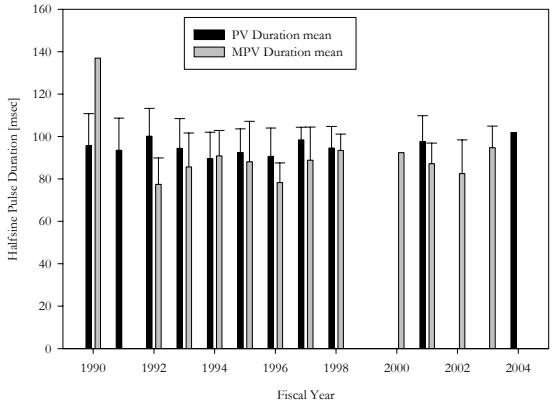

Figure 9. Mean and standard deviations of half sine durations per fiscal year for FMVSS 208 dynamic tests.

For the passenger vehicle classification the population peak defection, equivalent half sine acceleration pulse amplitude, equivalent half sine acceleration pulse circular frequency and equivalent half sine acceleration pulse duration were (mean ± SD) 0.619 ± 0.089 meters, 224.98 ± 30.39 m/sec^2, 34.11 ± 4.57 sec^{-1} and 94 ± 13 msec respectively. For the multi purpose vehicle classification the population valuations of these parameters were (mean ± SD) 0.557 ± 0.100 meters, 246.17 ± 43.61 m/sec^2, 37.78 ± 6.38 sec^{-1} and 86 ± 15 msec respectively. It should be noted that the mean value provided for the half sine pulse duration is a parameter determined from the population of the individual tests and is not an explicit implementation of equation (19) with the circular frequency assigned as being mean population value. The differences in the population means for all parameters between the passenger vehicle and multi-purpose vehicle classification were significant ($p < 0.00004$). Given the dearth of FMVSS 208 dynamic test data for fiscal years including and subsequent to 1997, a multiple comparison ANOVA analysis based upon each individual year being treated as a factor could not be conducted. A stratified regression analysis based upon test vehicle classification and test vehicle fiscal year with respect to the first fiscal year for which the alternative sled protocol was utilized (coded as an indexed variable) revealed a statistically significant difference ($p = 0.024$) for the equivalent half sine acceleration pulse amplitude for multi-purpose vehicles (pre-sled test implementation: 252.20 ± 44.55 m/sec^2, N = 53; post-sled test implementation: 223.32 ± 31.75 sec^{-1}, N = 14).

Pooled Dynamic Dataset

The population means of the relevant parameters between the set of FMVSS 208 dynamic and the set of tests not conducted under FMVSS 208 contract but having substantial similarity in accordance with the requirements set forth in the *Methods* section were compared prior to performing an analysis on the joint dataset. A segregated single factor ANOVA analysis was conducted for passenger vehicles and multi-purpose vehicles separately. The differences in the means between the FMVSS 208 dynamic and non-FMVSS 208 tests for the equivalent half sine acceleration pulse amplitude, equivalent half sine acceleration pulse circular frequency and equivalent half sine acceleration pulse duration were not significant ($p > 0.13$) for both passenger vehicles and multi-purpose vehicles except for the peak deflection parameter for passenger vehicles ($p=0.023$). The peak deflection for tests conducted under FMVSS 208 dynamic and for those not conducted under the same were 0.619 ± 0.089 meters ($N=191$) and 0.590 ± 0.062 meters ($N=58$) respectively. The means and standard deviations for the peak deflection, equivalent half sine acceleration pulse amplitude, circular frequency and pulse duration for the combined dataset are shown on a per fiscal year and vehicle category basis in Figures 10-13.

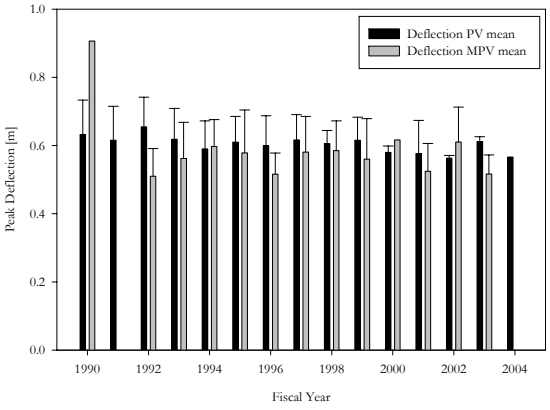

Figure 10. Means and standard deviations of peak deflections per fiscal year for the combined dynamic test database following categorization.

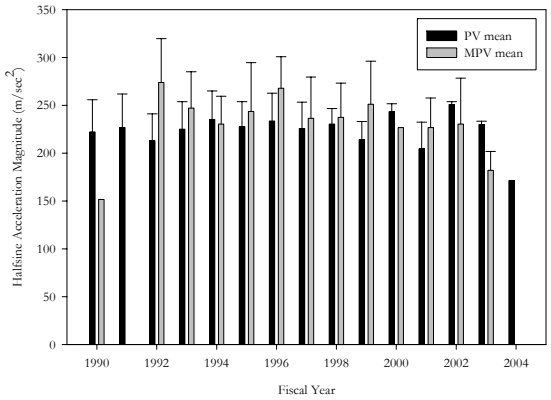

Figure 11. Mean and standard deviations of half sine acceleration amplitudes per fiscal year for the combined dynamic tests database following categorization.

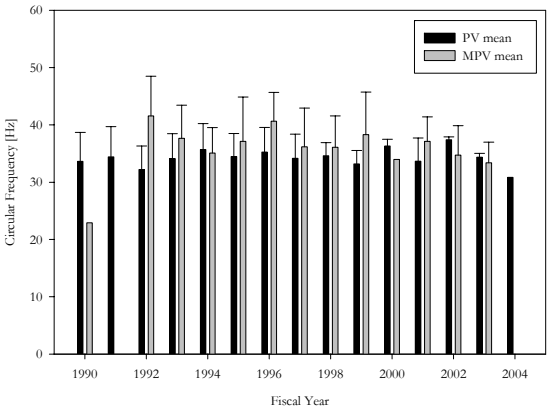

Figure 12. Means and standard deviations of half sine circular frequencies per fiscal year for the combined dynamic test database following categorization.

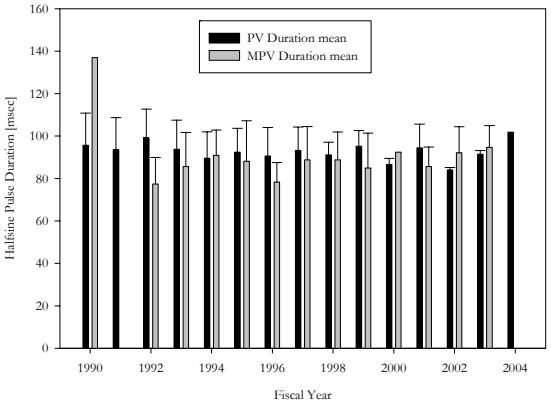

Figure 13. Mean and standard deviations of half sine pulse durations per fiscal year for the combined dynamic test database following categorization.

For the passenger vehicle classification, the valuations of these parameters for the entire dynamic dataset were 0.612 ± 0.085 meters, 225.10 ± 29.07 m/sec^2, 34.26 ± 4.26 sec^{-1} and 93 ± 12 msec respectively. For the multi-purpose vehicle classification, the valuations of these parameter for the entire dynamic dataset were 0.560 ± 0.102 meters, 243.82 ± 43.37 m/sec^2, 37.50 ± 6.28 sec^{-1} and 86 ± 15 msec respectively. There were no significant differences noted for any of these parameters for each vehicle classification for vehicles tested prior to the utilization of the alternative sled test protocol and subsequent to the same ($p > 0.18$) except for the equivalent half sine amplitude for the multi purpose vehicle classification ($p = 0.038$). The equivalent half sine amplitude for multi purpose vehicles tested prior to and subsequent to the inception of the alternative sled test protocol were 252.20 ± 44.55 m/sec^2 (N = 53) and 234.17 ± 40.31 m/sec^2 (N = 46) respectively. The differences in these parameters were significant when compared between passenger vehicles and multi purpose vehicles ($p < 0.0001$ for all parameters).

FMVSS 208 Sled Tests

The sled tests *en toto* generally followed the confines of the established maximum/minimum trapezoidal deceleration corridors. The results of the sled tests, shown per fiscal year conducted, plotted against the acceleration corridors and the target half sine pulse are shown in Figures 14-19.

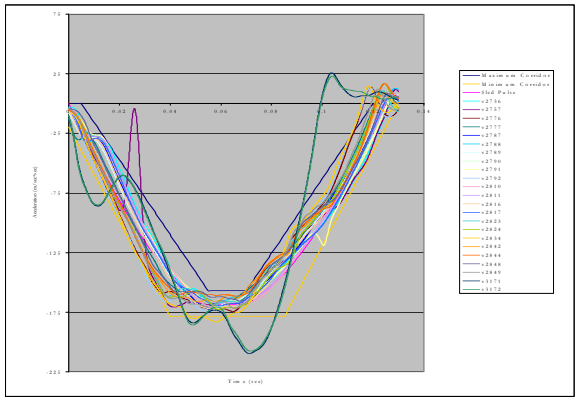

Figure 14. FMVSS 208 sled tests conducted for fiscal year 1998 overlayed on the acceleration corridors and idealized target half sine pulse.

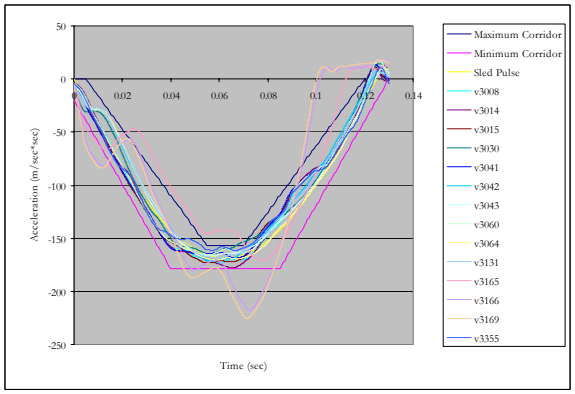

Figure 15. FMVSS 208 sled tests conducted for fiscal year 1999 overlayed on the acceleration corridors and idealized target half sine pulse.

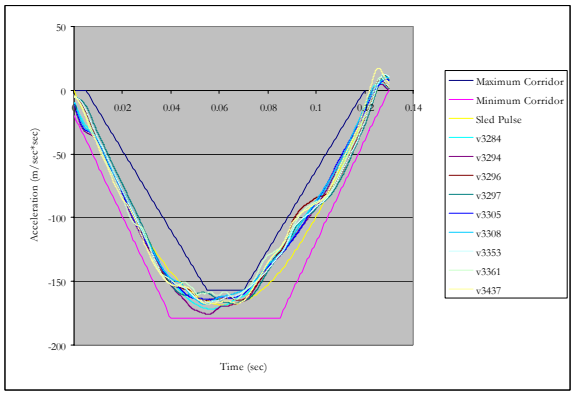

Figure 16. FMVSS 208 sled tests conducted for fiscal year 2000 overlayed on the acceleration corridors and idealized target half sine pulse.

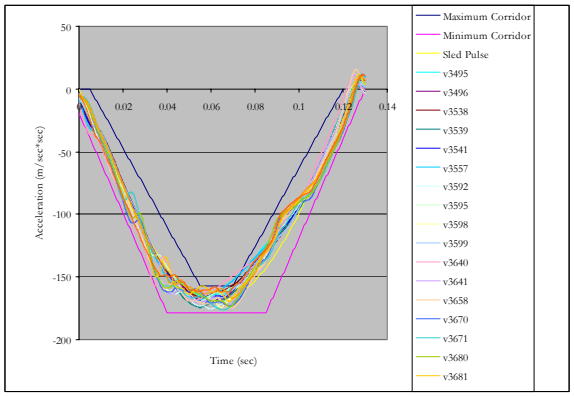

Figure 17. FMVSS 208 sled tests conducted for fiscal year 2001 overlayed on the acceleration corridors and idealized target half sine pulse.

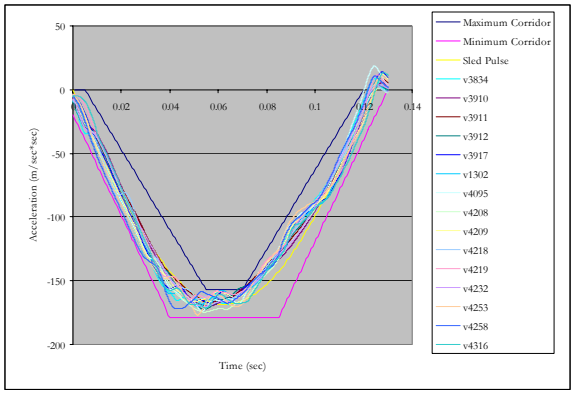

Figure 18. FMVSS 208 sled tests conducted for fiscal year 2002 overlayed on the acceleration corridors and idealized target half sine pulse.

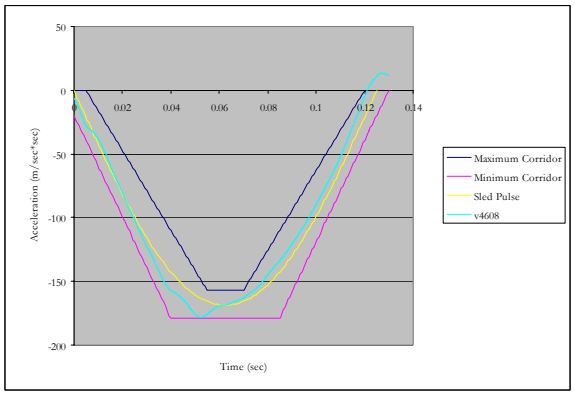

Figure 19. FMVSS 208 sled tests conducted for fiscal year 2003 overlayed on the acceleration corridors and idealized target half sine pulse.

Specific tests, as referenced within the figures, revealed significant deviations from the acceptable corridors for the first two years of implementation of the sled testing protocol. The underlying basis for these deviations, while being unclear from an analysis of the data alone, appeared to have been mitigated for sled tests conducted for fiscal years 2000 through 2003. Another class of deviation from the acceptable corridors, again cited on a test-specific basis in the figures, consisted of undershooting the segment of the maximum corridor in the vicinity of the transition from the plateau deceleration to the linearly decreasing region at approximately 70 msec.

DISCUSSION

An examination of Figure 3 reveals a significant drop in the total number of FMVSS 208 dynamic tests available for model years subsequent to fiscal year 1996 when compared to fiscal years 1990 through 1996. A total of zero tests were available for a number of years (1999, 2005) whereas other years during this range contained either only one (2000, 2004) or two tests (2002, 2003). Furthermore, the alternative sled test procedure was utilized for the majority of vehicles tested under FMVSS 208 for fiscal years 1998 through 2002. Therefore, the frontal impact response and actual frontal supplemental restraint system timing for the majority of vehicles tested for frontal impact compliance for these years remains unknown with an exception noted for the subpopulation of sled tested vehicles also tested under similar conditions for research, compliance procedure development and for the NCAP. A relevant issue, which unfortunately can not be addressed based on the subject data alone, is whether or not the dearth of dynamic frontal impact compliance data is secondary to the number of tests actually conducted or secondary to availability of test data released by the OCR.

In the ideal scenario it would have been preferable to have vehicle specific tests conducted in a pairwise manner with one test being conducted under the dynamic test protocol and the other being conducted under the sled test protocol. This would have allowed for a direct comparison of both the injury metrics and the characteristics of the deceleration pulse as a function of test protocol. The data from such testing, if it was in fact conducted, is not generally available. Even excluding this factor, the potential differences between the actual vehicle specific frontal supplemental restraint system timing and the imposed uniformed time of deployment of the frontal supplemental restraint system under the sled test protocol would render ineffective any comparison between the two protocols based upon injury metrics. As a result, the comparison between the population based characteristic deceleration pulses and the subject sled deceleration pulse was deemed as being the only satisfactory method for comparing the severity of each protocol. The equivalent half sine collision pulse model from dynamic test data was employed secondary to the use of the half sine pulse for the alternative sled test.

The half sine is the characteristic response of the single lumped mass linear spring model subject to the dissipative force and initial conditions as described in the *Introduction*. This model, while being appropriate for field and reconstructive studies in that the parameter of interest in these studies is the directional vehicle change in speed, has limitations for modeling the detailed deceleration response for FMVSS 208 dynamic collision tests. The limitation arises from the inability of the subject SDOF model to replicate the local extrema of the acceleration-time history that characterize test data obtained from

actual impact testing. The acceleration-time history of NHTSA test v2463 as shown in Figure 5 is characteristic of this phenomenon and was observed for the subject data *en toto*. This response is characteristic, from a uniaxial modeling perspective, of the multiple lumped mass nature of current vehicle frontal structures. The various local extrema, which are also observable as peaks in the total barrier force response from New Car Assessment Program (NCAP) tests, are secondary to impulsive deceleration and shortening of the vehicle frontal structure, engine and vehicle structures between the engine and firewall [Wood and Mooney, 1997]. The use of the SDOF response, and thereby model, implies appropriateness for characterization of the relevant aspects of the collision pulse. Within this context, the SDOF model can be fitted to match the uniaxial change in speed (to zero) and time duration of the actual deceleration pulse.

Hollowell et al., [1998, 1999], in their evaluation of potential compliance tests for frontal impact collision protection, characterized deceleration pulses based upon the acceleration levels and pulse durations. Testing modalities that had low acceleration levels and long pulse durations were characterized as being soft whereas those with high acceleration levels and short pulse durations were characterized as being stiff. While specific quantitative guidelines were not proposed for these qualitative descriptors it was noted that on the basis of average acceleration and pulse duration that a substantial difference was noted between the FMVSS 208 dataset from 1990-1998 and the FMVSS 208 sled test deceleration pulse. The findings of the subject study, consistent with the cited prior studies, do reveal a substantive difference between the sled pulse and the equivalent half sine approximation mean response of the population of vehicles tested dynamically. The response characteristics of vehicles tested dynamically under FMVSS 208, vehicles tested dynamically under conditions substantially similar to FMVSS 208 and the idealized sled pulse in terms of the half sine acceleration, pulse amplitude, circular frequency, duration and the corresponding displacement are shown in Table 1.

Table 1.
Impact and sled test characteristics

Test Type	A_p (m/sec^2)	ω_n (sec^{-1})	T_{impact} (sec)	Deflection (m)
208D	230.49 ± 35. 57	35.06 ± 5.38	92 ± 14	0.603 ± 0.096
Research	230.43 ± 34.75	35.18 ± 5.12	91 ± 13	0.598 ± 0.092
208S	168.73	25.13	125	0.839

The finding of significant differences in the equivalent half sine parameters between passenger vehicles and multi-purpose vehicles is indicative of the generally stiffer response of the latter. This finding is consistent with prior studies [Hollowell and Gabler, 1996; Gabler and Hollowell, 1998].

The lack of equivalence between the equivalent half sine parameter quantification proposed by Huang [2002] and that based upon the modified methodology of Varat and Husher [2003] is an unexpected finding in that the formulation of the former reduce to that of the latter with the explicit imposition of the boundary constraints and substitution of the definition of the circular frequency in terms of the impact duration. In that consistency was noted between the two formulations in regards to quantification of the half sine parameters, the differences in the results can not be attributed to miscoding of the algorithms proposed by Huang [2002]. A further evaluation is needed to determine the underlying source of the differences in the two algorithms for those tests in which the same result was not determined.

CONCLUSIONS

The quantitative parameterization of the half sine pulse utilized for the FMVSS 208 sled test substantially underestimates the mean equivalent half sine approximation response for both passenger vehicles and multipurpose vehicles tested under FMVSS 208 dynamic and substantially similar barrier impact modalities.

REFERENCES

Gabler, H.C. and W.T. Hollowell. 1998. "The Aggressivity of Light Trucks and Vans in Traffic Crashes." Society of Automotive Engineers Technical Paper Series 980908.

Hollowell, W.T. and H.C. Gabler. 1996. "NHTSA's Vehicle Aggressivity and Compatibility Research Program." Proceedings: 15th International Conference on the Enhanced Safety of Vehicles. Paper No. 96-S4-O-01. Melbourne, Australia.

Hollowell, W.T., H.C. Gabler, S.L. Stucki, S. Summers, J.R. Hackney. 1998. Review of Potential Test Procedures for FMVSS No. 208. United States Department of Transportation. National Highway Safety Administration. Office of Vehicle Safety Research.

Hollowell, W.T., H.C. Gabler, S.L. Stucki, S. Summers and J.R. Hackney. 1999. Updated Review of Potential Test Procedures for FMVSS No. 208. United States Department of Transportation. National Highway Safety Administration. Office of Vehicle Safety Research.

Huang, M. 2002. Vehicle Crash Mechanics. CRC Press; Boca Raton, Florida, USA.

United States Department of Transportation. National Highway Traffic Safety Administration. Office of Vehicle Safety Compliance: Safety Assurance. Laboratory Test Procedure for FMVSS 208, Occupant Crash Protection Sled Tests. TP208S-01. January 15, 1998.

United States Department of Transportation. National Highway Traffic Safety Administration. Office of Vehicle Safety Compliance: Enforcement. Laboratory Test Procedure for FMVSS 208, Occupant Crash Protection; FMVSS 212, Windshield Mounting; FMVSS 219, Windshield Zone Intrusion; FMVSS 301F, Fuel System Integrity – Frontal. TP208-12. January 14, 2003.

Varat, M. and S. Husher. 2003. "Crash Pulse Modeling for Vehicle Safety Research." Proceedings: 18th International Technical Conference on the Enhanced Safety of Vehicles. Nagoya, Japan.

Wood, D.P. and S. Mooney. 1997. "Modeling of Car Dynamic Frontal Crush." Society of Automotive Engineers Technical Paper Series 970943.

APPENDIX A

The general form of a half sine pulse as a function of peak amplitude *A*, pulse duration *T* and time shift τ is given by equation (A1).

$$\ddot{x}(t) = A_p \cdot \sin\left(\frac{\pi \cdot (t-\tau)}{T}\right) \qquad \text{(A1).}$$

The closest approximating ideal half sine pulse that is admissible in regards to the maximum trapezoidal corridor is determinable by enforcement of the acceleration values at the start and end of the maximum corridor plateau.

$$\ddot{x}(t=0.055) = -156.96 = A_p \cdot \sin\left(\frac{\pi \cdot (0.055-\tau)}{T}\right) \qquad \text{(A2).}$$

$$\ddot{x}(t=0.070) = -156.96 = A_p \cdot \sin\left(\frac{\pi \cdot (0.070-\tau)}{T}\right) \qquad \text{(A3).}$$

Equating equations (A2) and (A3) with the substitution of τ = 0.005 seconds and solving for the pulse duration *T* results in *T* = 0.115 seconds. Substitution of this solution into equation (A2) results in the solution for the amplitude as being A_p = -160.313 m/sec^2. Therefore the equation for the closest approximating ideal half sine pulse that is admissible based upon the requirements of the maximum corridor is:

$$\ddot{x}(t) = -160.313 \cdot \sin\left(\frac{\pi \cdot (t-0.005)}{0.115}\right) \qquad \text{(A4).}$$

Equation (A4) is valid temporally over the region {t: 0.005 sec ≤ t ≤ 0.120 sec}. Explicit integration of equation (A4) over this duration results in a uniaxial change in speed of - 11.737 m/sec (-26.255 MPH). Implicit integration of equation (A1) results in the solution for the velocity.

$$\dot{x}(t) = \frac{A_p \cdot T}{\pi} \cdot \cos\left(\frac{\pi \cdot (t-\tau)}{T}\right) + c_1 \qquad \text{(A5).}$$

For the FMVSS 208 sled test, the constant of integration c_1 can be determined by substitution of the initial condition $\dot{x}(0) = 0$ into equation (A5).

$$c_1 = -\frac{A_p \cdot T}{\pi} \cdot \cos\left(-\frac{\pi \cdot \tau}{T}\right) \qquad \text{(A6).}$$

Substitution of equation (A6) into equation (A5) and implicitly integrating the results in the displacement solution.

$$x(t) = \frac{A_p \cdot T}{\pi} \cdot \left[\begin{array}{l} -t \cdot \cos\left(\frac{\pi \cdot t}{T}\right) + \\ \frac{T}{\pi} \cdot \sin\left(\frac{\pi \cdot (t-\tau)}{T}\right) \end{array}\right] \qquad \text{(A7).}$$

Explicit integration of the velocity solution over the appropriate temporal limits of integration results in a solution for the total displacement of -0.669 meters (-26.3 inches) that occurs over the pulse duration.

The closest approximating half sine pulse that is admissible in regards to the minimum trapezoidal corridor is determined by first noting that pulse duration must equal 0.130 + (2 / 0.405) * 10^{-3} seconds and that the time-shift is - (2 / 0.405) * 10^{-3} seconds. The amplitude can be determined by noting that the first time derivative of the half sine acceleration pulse (i.e. the jerk) must be less than or equal to the first time derivative of the rising leg of the trapezoidal deceleration bounding function over {t: -(2 / 0.405) * 10^{-3} ≤ t < 0.040 seconds}. Enforcement of the equality constraint between the two time derivatives at the lower time limit results in the following relationship where the period and the time-shift are in units of msec and the constant term on the right of the second equality is in units of G/msec:

$$\dddot{x}(0) = \frac{A_p \pi}{T} \cdot \cos\left(\frac{\pi \cdot (0 - \tau)}{T}\right) = -0.405 \qquad \text{(A8).}$$

The solution for the amplitude is A_p = -170.651 m/sec^2. The solution for the half sine pulse thus becomes:

$$\dddot{x}(t) = -170.651 \cdot \sin\left(\frac{\pi \cdot \left(t - \left(\frac{2}{0.405}\right) \cdot 10^{-3}\right)}{\left(120 + \frac{2}{0.405}\right) \cdot 10^{-3}}\right) \qquad \text{(A9).}$$

Explicit integration of equation (A9) over the temporal limits results in a uniaxial change in speed of - 13.365 m/sec (- 29.897 MPH). Explicit integration of equation (A5) following substitution of the appropriate definitions for the amplitude, time-shift and duration results in a displacement of -0.983 meters (-38.7 inches).

APPENDIX B

The displacement solution to the second order differential equation of motion of equation (2) is determinable by the sum of the homogenous and particular solutions.

$$\begin{aligned} &x(t) = x_h(t) + x_p(t) = \\ &A \cdot Cos(\omega_n \cdot t) + B \cdot Sin(\omega_n \cdot t) + C \cdot t \end{aligned} \qquad \text{(B1).}$$

The coefficients *A*, *B* and *C* can be determined from the system initial and boundary conditions. Substitution of the initial displacement condition into equation (B1) results in the solution of A = 0.

$$\begin{aligned} &x(0) = 0 = \\ &A \cdot Cos(\omega_n \cdot 0) + B \cdot Sin(\omega_n \cdot 0) + C \cdot 0 \rightarrow 0 = \\ &A \cdot 1 \rightarrow A = 0 \end{aligned} \qquad \text{(B2).}$$

The velocity solution is obtained by taking the first time derivative of equation (B1) following substitution of equation (B2) for the coefficient *A*.

$$\dot{x}(t) = B \cdot \omega_n \cdot Cos(\omega_n \cdot t) + C \qquad \text{(B3).}$$

The period of the waveform is related to the circular frequency of the sinusoid by equation (B4).

$$\omega_n = \frac{2\pi}{T_{period}} \qquad \text{(B4).}$$

Substitution of equation (B4) into the velocity solution of equation (B3) results in the following:

$$\dot{x}(t) = \frac{2 \cdot \pi \cdot B}{T_{period}} \cdot Cos\left(\frac{2 \cdot \pi \cdot t}{T_{period}}\right) + C \qquad \text{(B5).}$$

The coefficients *B* and *C* can be solved for simultaneously by implementing the initial condition for the velocity of $\dot{x}(0) = v_o$ and the desired boundary condition of $\dot{x}\left(\frac{T_{period}}{2}\right) = 0$.

$$\begin{aligned} &\dot{x}\left(\frac{T_{period}}{2}\right) = 0 = \\ &\frac{2 \cdot \pi \cdot B}{T_{period}} \cdot Cos\left(\frac{2 \cdot \pi \cdot T_{period}}{2 \cdot T_{period}}\right) + C \rightarrow 0 = \\ &\frac{2 \cdot \pi \cdot B}{T_{period}} \cdot Cos(\pi) + C \rightarrow C = \frac{2 \cdot \pi \cdot B}{T_{period}} \end{aligned} \qquad \text{(B6).}$$

$$\begin{aligned} &v_o = \frac{2 \cdot \pi \cdot B}{T_{period}} + C \rightarrow v_o = \\ &\frac{2 \cdot \pi \cdot B}{T_{period}} + \frac{2 \cdot \pi \cdot B}{T_{period}} \rightarrow B = \frac{v_o \cdot T_{period}}{4 \cdot \pi} \end{aligned} \qquad \text{(B7).}$$

$$C = \frac{2 \cdot \pi \cdot B}{T_{period}} \rightarrow \frac{2 \cdot \pi \cdot v_o \cdot T_{period}}{4 \cdot \pi \cdot T_{period}} \rightarrow \frac{v_o}{2} \qquad \text{(B8).}$$

Substitution of the definition of *B* from equation (B7) and *C* from equation (B8) into the

solutions for the displacement, velocity and acceleration result in the following:

$$x(t) = \frac{v_o \cdot T_{period}}{4 \cdot \pi} \cdot Sin\left(\frac{2 \cdot \pi \cdot t}{T_{period}}\right) + \frac{v_o}{2} \cdot t \qquad \text{(B9).}$$

$$\dot{x}(t) = \frac{v_o}{2} \cdot Cos\left(\frac{2 \cdot \pi \cdot t}{T_{period}}\right) + \frac{v_o}{2} \qquad \text{(B10).}$$

$$\ddot{x}(t) = -\frac{v_o \cdot \pi}{T_{period}} \cdot Sin\left(\frac{2 \cdot \pi \cdot t}{T_{period}}\right) \qquad \text{(B11).}$$

The half sine pulse employs only half of the full period. Using the relationship of $T_{period} = 2 * T_{impact}$, equations (B9-B11) can be rewritten as:

$$x(t) = \frac{v_o \cdot T_{impact}}{2 \cdot \pi} \cdot Sin\left(\frac{\pi \cdot t}{T_{impact}}\right) + \frac{v_o}{2} \cdot t \qquad \text{(B12).}$$

$$\dot{x}(t) = \frac{v_o}{2} \cdot Cos\left(\frac{\pi \cdot t}{T_{impact}}\right) + \frac{v_o}{2} \qquad \text{(B13).}$$

$$\ddot{x}(t) = -\frac{v_o \cdot \pi}{2 \cdot T_{impact}} \cdot Sin\left(\frac{\pi \cdot t}{T_{impact}}\right) \qquad \text{(B14).}$$

MECHANICAL MODELS OF CELLULAR SOLIDS, PARAMETERS IDENTIFICATION FROM EXPERIMENTAL TESTS

Massimiliano Avalle
Giovanni Belingardi
Andrea Ibba
Dipartimento di Meccanica, Politecnico di Torino
Italy
Paper Number 05-0438

ABSTRACT

Cellular solids are largely used in many structural applications to absorb and dissipate energy, due to their light weight and high energy absorption capability.

The appropriate design of mechanical pieces made of structural foams must be done on the basis of the kind of impact, the energy involved and the maximum admissible stress. In the design development it is of highest importance the choice of the proper type of foam at the proper density level. This is based on stress-strain behaviour that can be predicted by means of test curves and models.

The parameters of two cellular solids models for EPP, PUR, EPS and NORYL GTX foams have been identified by means of experimental compression tests at different densities. The Gibson model and a modified version of this model have been considered: the fitting of these models are compared also with the Rusch model and a modified version of the Rusch model.

The considered models are directly derived from theoretical micro-mechanical assumptions while the parameter values are identified by means of the available experimental data.

Model parameters depend on the foam density and a mathematical formulation of this dependence is identified.

The formulas of the density dependence of the model parameters permits the identification of all foams made starting from the same solid material and with the same micro-structure by means of a minimum set of experimental tests. At the same time the availability of a large quantity of experimental data allows to reach a higher confidence level for the model parameters values.

The identified laws that describe parameters against density, for a certain type of foam, could be used in order to assist the design of the absorber and to find the optimum density for the specific application.

1. INTRODUCTION

The increasing request of more performing and safer vehicles has given great importance to cellular solid materials in automotive industry. This kind of materials is successfully used in vehicles in order to minimise the weight of structural components and to improve the safety through the absorption of impact energy in crash events.

In this second type of application cellular solids are used to absorb impacts between vehicle and external obstacles and the consequent internal impacts of the passengers against the body structure of the vehicle. In both cases cellular solid components should be designed in order to control the deceleration of the impacting parts (vehicle or passengers) and in order to limit its maximum value. For this aim cellular solids are very functional and permit the design of a component to meet the exact requirements for a specific impact. The mechanical characteristics can be modulated in a continuous way acting on the density and on the micro-structure besides on the constitutive material: it is possible to integrate the design of the proper mechanical characteristics with the design of shape and dimensions of the component.

This functionality implies more complexity in design computation. It could be very onerous to characterise and identify all cellular solids which can be used for a specific application and it could be onerous to analyse the behaviour of each of them.

For design purposes a unified modelisation of a larger set of materials identified with less experimental testing could be very helpful. A unique model for cellular solids made of the same constitutive material and for a wide range of density could be used to direct the choice of the optimal foam density for defined impact energy absorption. Moreover it can be used in FEM crash simulations in order to analyse the behaviour of different foams, also experimentally not tested. The aim of this work is the analysis and development of these features on cellular solids modelisation.

Experimental testing on four types of foams have been analysed and different models have been identified and compared by means of these experimental data.

The variation of model parameters with foam density has been studied in order to develop parameters-density laws to be integrated in each model.

2. EXPERIMENTAL TESTS

Static uniaxial compression tests, made according with ASTM D1621-94 (*Standard Test Method for Compressive Properties of Rigid Cellular Plastics*) have been performed on different kinds of foams at different densities:

- **Expanded polypropylene** foams (EPP) tested at five different nominal densities with a wide range of variation: 31, 45, 70, 106 and 145 g/dm^3.
- **Expanded polystyrene** foams (EPS) tested at four different nominal densities, but the range of variation is relative narrow: 40, 50, 60 and 70 g/dm^3.
- **Expanded polyurethane** foams (PUR) tested only at two different densities: 70 and 100 g/dm^3.
- **Noryl GTX** foams, tested at two different densities: 50 and 75 g/dm^3.

All specimens were cubic with 50 mm side, except for the expanded polystyrene specimens which were cylindrical with a diameter of 100 mm and height of 35 mm. Each specimen was previously weighted and measured in order to calculate its effective density. The tests consist of the compression of the foam specimen between two rigid steel plates at a constant relative velocity of 60 mm/min, which corresponds to a strain rate of 2×10^{-2} s^{-1}. The maximum stroke chosen is 90% of the initial thickness. A hydraulic universal testing machine (DARTEC 9600) was used; the piston displacement and the force were measured at an appropriate sampling frequency. For each nominal density of each kind of foam at least three repetitions of the compression test were performed.

3. CELLULAR SOLIDS MODELS

Cellular solids models can be divided in two categories: phenomenological model and micro-mechanical models. The phenomenological models aim to reach the best fit with the experimental mechanical behaviour without direct relationship with the physics of the phenomenon. The micro-mechanical models are based on the analysis of the deformation mechanisms of the micro-cell structure under loading.

The micromechanical Gibson model and a proposed modified Gibson model have been identified for all tested materials. Their fitting capability has been compared with the phenomenological Rusch model and a modified Rusch model already identified for the same foams in [6].

3.1 Gibson Model

The most known and widely used micro-mechanical model is the Gibson model (Gibson, Ashby [1]) in which the stress-strain compression curve is split into three parts (elastic, collapse and densification) and analytical relationship are obtained. The behaviour is mainly controlled by the relative density of the foam with respect to the solid base material.

The formulations of the three regions are:

- Linear elastic region:

$$\sigma = E\varepsilon \qquad (1a)$$

$$\text{if } \sigma \le \sigma_{yield} \qquad (1b)$$

- Plateau region:

$$\sigma = \sigma_{yield} \qquad (2a)$$

$$\text{If } \varepsilon_{yield} \le \varepsilon \le \varepsilon_D\left(1 - D^{-1/m}\right) \qquad (2b)$$

- Densification region:

$$\sigma = \sigma_{yield}\,\frac{1}{D}\left(\frac{\varepsilon_D}{\varepsilon_D - \varepsilon}\right)^m \qquad (3a)$$

$$\text{if } \varepsilon > \varepsilon_D\left(1 - D^{-1/m}\right) \qquad (3b)$$

The model has five parameters and each of them can be calculated by means of author's dedicated formulas based on the micro-mechanics of foam deformation. In this work the parameters have been identified on the basis of the experimental curves so that the identified values can be compared to the theoretical ones. The parameters E, σ_{yield} and ε_D are considered density dependent, while D and m should be density independent.

3.2 Modified Gibson Model

The original Gibson model has been modified in order to test the possibility to improve its fitting capability. A sloped linear model is proposed instead

of a constant stress model for the modelling of the plateau region. The equation (2a) is substituted by the following expression:

$$\sigma = \sigma_{yield} + h\varepsilon \qquad (4)$$

This modification implies the identification of two parameters instead of a single one for this region, and a total of 6 parameters for the whole model.

The strain value of the intersection between the plateau region and the densification region can not be expressed explicitly as in the original Gibson model: it must be found numerically.

3.3 Rusch Model and Modified Rusch Model

A simpler and effective phenomenological model is the Rusch model (Rusch [2], [3] and [4]). It had been extensively tested in previous works of the authors (Avalle, Belingardi, Ibba [6]) and it demonstrated a good fitting capability combined to some advantages in the identification process with respect to the Gibson model.

A modification of the model had also been proposed in order to improve the fitting capability in the densification region. Both models had been identified in [6] for the same foams analysed here.

The Rusch model is a phenomenological model having a simple formulation, described by the sum of two power laws:

$$\sigma = A\varepsilon^m + B\varepsilon^n \qquad (5a)$$

$$\text{with } 0 < m < 1,\ 1 < n < \infty \qquad (5b)$$

ε is engineering strain and is considered positive in compression. The first addendum is used to fit the elastic-plateau region, while the second addendum is used to model the densification region. The parameters *A* and *B* are considered density dependent, while *m* and *n* are not.

The modified version of the Rusch model, proposed in [6], had been developed in order to improve the fit in the densification region. The second addendum is modified in order to have a vertical asymptote at the physical limit of compression strain:

$$\sigma = A\varepsilon^m + B\left(\frac{\varepsilon}{1-\varepsilon}\right)^n \qquad (6a)$$

$$\text{with } 0 < m < 1 \text{ and } 1 < n < \infty \qquad (6b)$$

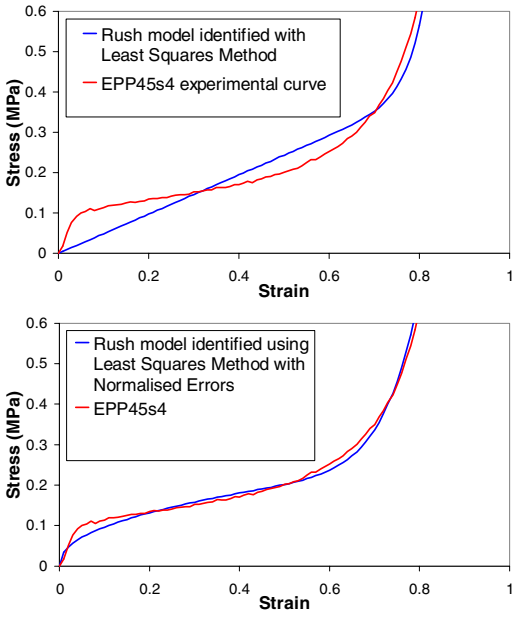

Figure 1. Comparison between the models identified with the least squares method using the squared errors and the normalised squared errors. Five densities of EPP foams have been identified at the same time.

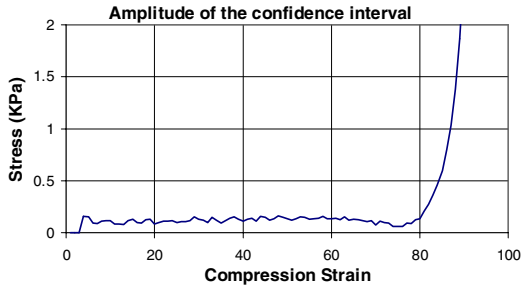

Figure 2. Amplitude of the confidence interval versus strain.

4. IDENTIFICATION METHOD

Two procedures of parameters identification have been used in order to identify the material parameters, for each model:

1. The whole set of parameters of the models are identified for each experimental curve
2. Only the density dependent parameters are identified for each experimental curve, while the density independent parameters are identified on the whole set of curves together

The second identification procedure is more interesting because it allows to separate the density influence from the other material parameters and to evaluate their dependence from the density itself. The least squares method has been used to identify the material parameters. However, it gave poor results

when applied to the not weighted sum of the square errors, especially in the case of second procedure of identification. In fact, it suffers the over-weighted influence of the high density foams and vice versa. This is due to the fact that the gaps between experimental stress and model predicted stress of the low density foams are always low compared to the gaps of the higher density foams. Considering that the second kind of identification is obtained through the minimization of the sum of the square errors of all foam density curves, it is clear that the variation of the total sum due to the variation of the parameters of the low density foams is very little compared to the variation of the total sum due to the same relative variation of the parameters of the high density foams.

The identification based on plain sum of the square errors is too loose for low density foams at low strain (and stress). Therefore, the fitting has been performed by weighting the errors with the value of the experimentally measured stress. Hence, the sum of the normalised square errors (SNSE) to be minimised is:

$$SNSE = \sum_i \left(\frac{\sigma_{sper,i} - \sigma_{\mathrm{mod},i}}{\sigma_{sper,i}} \right)^2 \quad (7)$$

where $\sigma_{sper,i}$ and $\sigma_{mod,i}$ are the experimental stress and the model predicted stress respectively, corresponding to the same strain.

The normalised squares minimization procedure brings a better fit of the elastic and plateau regions although a slightly worse fit is obtained in the densification region (Figure 1).

The choice of the procedure based on the normalised least squares is justified by technical and statistical reasons.

In impact applications, the foam should absorb a defined quantity of energy with fixed maximum displacement and stress level. This goal can be achieved by taking advantage of the linear and plateau region: from a design point of view the prediction of the energy involved in the plateau region has a primary role. The use of the foam in the densification region is unlikely because the foam would absorb energy with rising stress and quickly rising tangent stiffness. Moreover different densities of the same type of foam could result in large differences of the plateau stress, so in the global identification of all model curves it is advantageous to evaluate the gaps between the experimental curves and the model curves in a relative way: the errors should be proportional to the stress level of each curve.

From a statistical point of view the lack of fit of the model must be evaluated weighting the effect of the variance of experimental data. The confidence intervals of the experimental stress values as function of the strain has been calculated by means of three repetitions of a test on the same foam. Figure 2 shows the remarkable quality of the fit in the elastic and plateau region and the enlargement of the confidence intervals only in the densification region.

5. COMPARISON OF MODELS PERFORMANCE

Performance of models can be visualised graphically by means of the stress-strain curves of identified models and experimental data. In Figures 3 and 4 the Gibson model and the modified Gibson model curves of the EPP at 70 g/l are shown, while in Figures 5 and 6 the Rusch model and the modified Rusch model identified in [6] for the same material are shown. All models seem to fit satisfactorily the experimental curves with an advantage for the Gibson type models. The difference between model stress and experimental stress (error) plotted as function of the strain is a better way to compare the fitting characteristics of models: these curves are shown for the same foam and the same models.

The identification has been performed with method 2 described in the previous paragraph. For this reason the fitting on each single curve is a little bit penalised by the need to have a unique identified value of the density independent parameters for the whole set of tested foams of the same type.

A quantitative comparison of the global fitting capability of the models has been performed by means of the total sum of the normalised square errors for each kind of foam (Fig. 7-10). The modified version of the Gibson model shows always the best fitting.

6. MODELS OF THE DENSITY EFFECT

The identified models have been further analysed in order to obtain the relationship between material density and model parameters and to develop laws describing this source of variation. In the Gibson model, as a micromechanical model, this relationship is an assumption of the model itself, which can be eventually verified by comparison with the parameters values identified by experimental data.

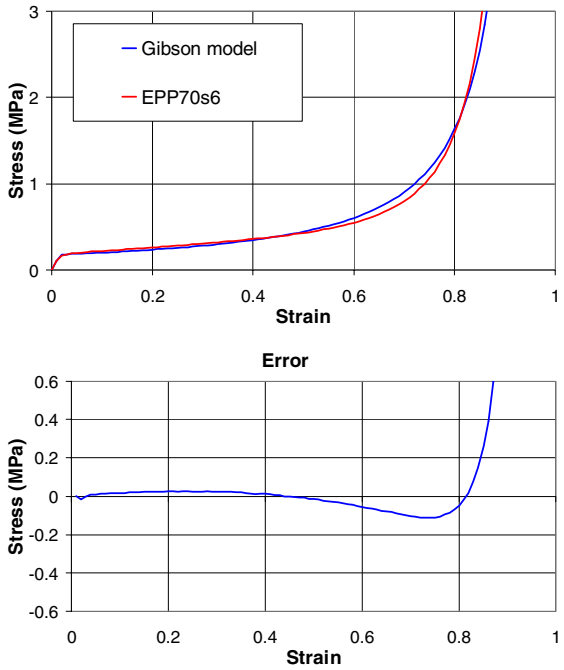

Figure 3. Experimental stress-strain curve of the EPP 70 g/l and the corresponding identified Gibson model curve.

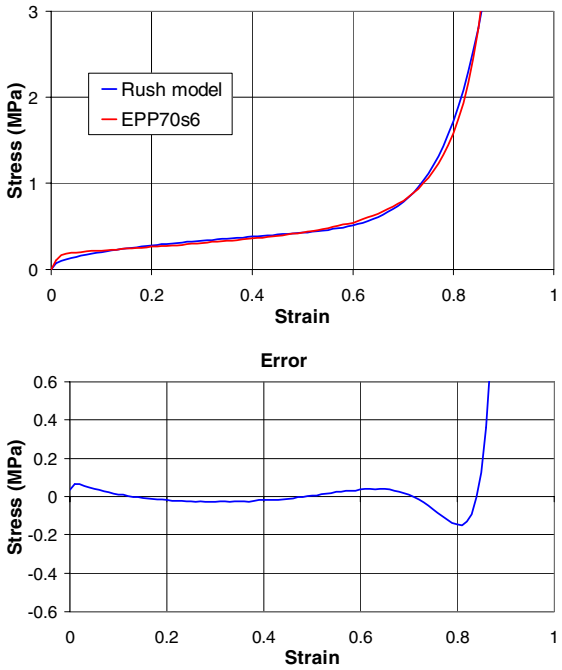

Figure 5. Experimental stress-strain curve of the EPP 70 g/l compared to the Rusch model with the identified parameters.

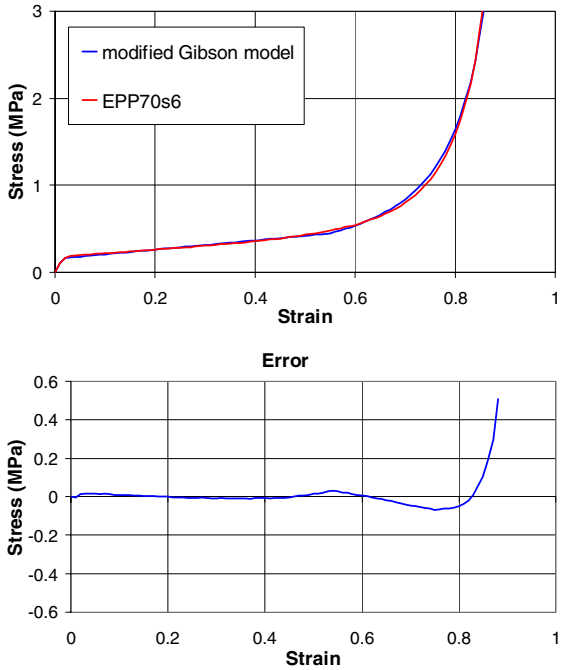

Figure 4. Experimental stress-strain curve of the EPP 70 g/l compared to the modified Gibson model with the identified parameters.

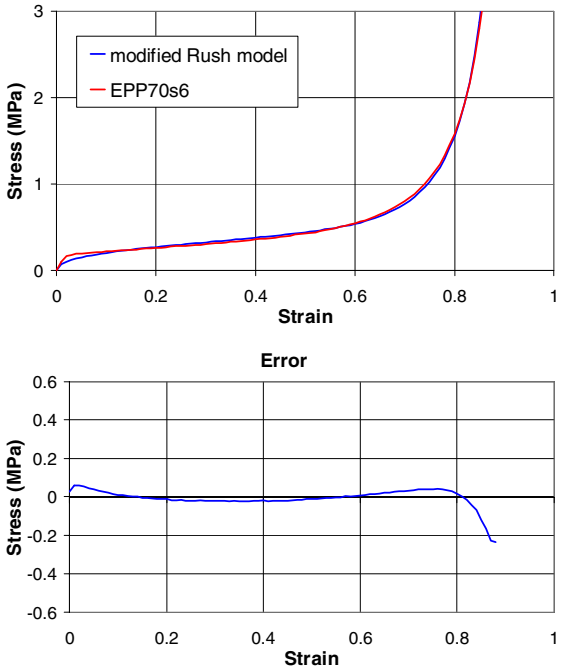

Figure 6. Experimental stress-strain curve of the EPP 70 g/l compared to the modified Rusch model with the identified parameters.

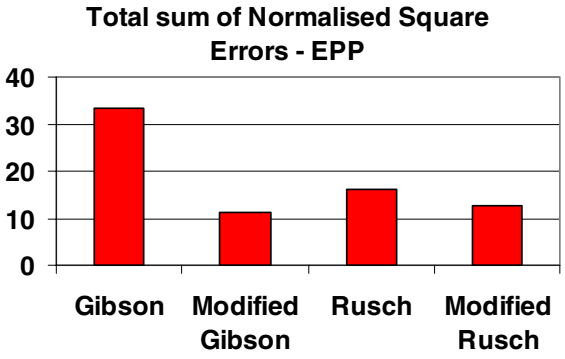

Figure 7. Comparison of the total sum of normalised square errors of the models identified for EPP foams.

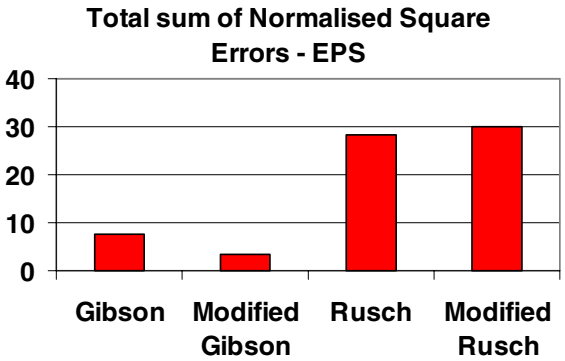

Figure 8. Comparison of the total sum of normalised square errors of the models identified for EPS foams.

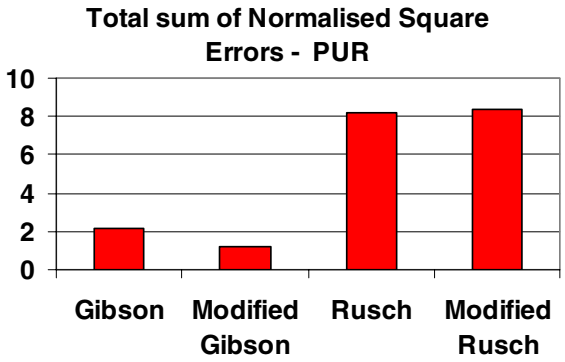

Figure 9. Comparison of the total sum of normalised square errors of the models identified for PUR foams.

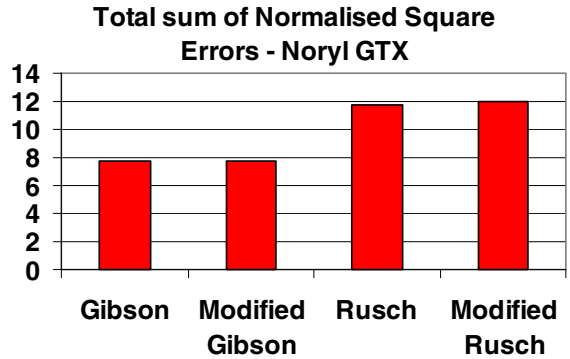

Figure 10. Comparison of the total sum of normalised square errors of the models identified for Noryl GTX foams

6.1 Gibson Model

The Gibson model includes the density effect on parameters as a consequence of the micromechanical deformation mechanisms which are on the basis of the model itself. It does not need experimental data in order to quantify it: the micromechanical theory is used.

This feature of the Gibson model is useful when few experimental data on the density effect are available. On the other hand the availability of some experimental data on foamed materials at different density levels should be useful to better fit the effective density effect. For this aim the structure of the Gibson parameters-density laws have been maintained but its parameters have been identified through the experimental data.

Elastic Modulus

In case of open cell foams the variation of the elastic modulus with density is modelled by Gibson with the following relation:

$$\frac{E}{E_S} \approx \left(\frac{\rho}{\rho_S}\right)^2 \qquad (8)$$

E, E_S, ρ and ρ_S are the elastic modulus of the foam, the elastic modulus of the solid material of which the foam is made, the density of the foam and the density of the solid material respectively.

The equation can be written with a parameter to be identified by means of the elastic moduli already identified for each tested foam density:

$$E = C_E \rho^2 \qquad (9)$$

In this relation the parameter C contains the ratio of the elastic modulus to the square density of the solid material corrected by a factor which permits to reach a better fit of the experimental data.

The experimentally identified elastic moduli for each specimen, the proposed relation, identified by means of these data, and the original Gibson relation are shown and compared in Figures 11-14 for each type of foam. Identified C_E values are in Table 1.

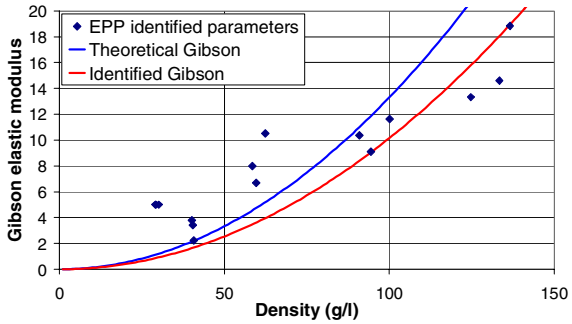

Figure 11. Gibson model for the EPP foams: identified elastic moduli, theoretical parameter-density relation and identified relation.

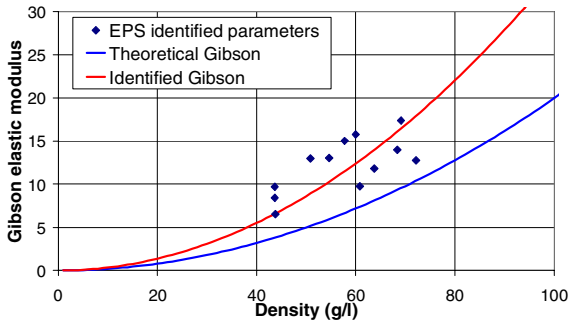

Figure 12. Gibson model for the EPS foams: identified elastic moduli, theoretical parameter-density relation and identified relation.

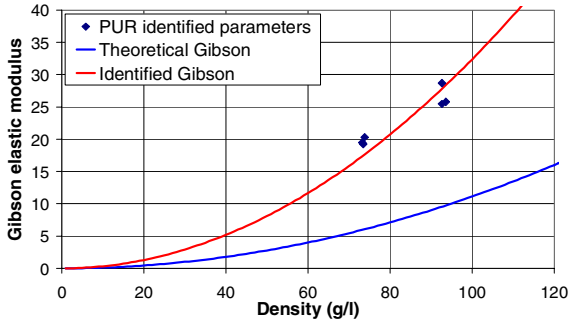

Figure 13. Gibson model for the PUR foams: identified elastic moduli, theoretical parameter-density relation and identified relation.

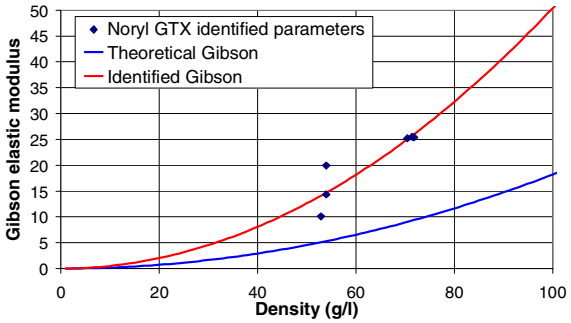

Figure 14. Gibson model for the Noryl GTX foams: identified elastic moduli, theoretical parameter-density relation and identified relation.

Yield Stress

For open cell foams with plastic collapse behaviour the variation of the plastic collapse stress with density is modelled by Gibson with the following relation:

$$\frac{\sigma_y}{\sigma_{yS}} \approx 0.3\left(\frac{\rho}{\rho_S}\right)^{\frac{3}{2}} \qquad (10)$$

σ_y and σ_{yS} are the plastic collapse stress of the foam and the yield stress of the solid material respectively. As made for the elastic modulus the equation can be written in the following form:

$$\sigma_y = C_y \rho^{\frac{3}{2}} \qquad (11)$$

The parameter can be identified through the experimentally identified plastic collapse stress for each tested foam. The identified plastic collapse stresses and the identified previous relations are shown in Figures 15-18 for each type of foam. Identified C_y values are in Table 1.

Densification Strain

For the densification strain parameter Gibson proposes the equation

$$\varepsilon_D = 1 - 1.4\left(\frac{\rho}{\rho_S}\right) \qquad (12)$$

This is not derived directly from micromechanical mechanisms; it is defined with a semi-empirical approach, so that the value 1.4 can be substituted by a constant to be identified:

$$\varepsilon_D = 1 - C_D \rho \qquad (13)$$

The identified densification strains and the identified previous relations are shown in Figures 19-22 for each type of foam. Identified C_D values are in Table 1.

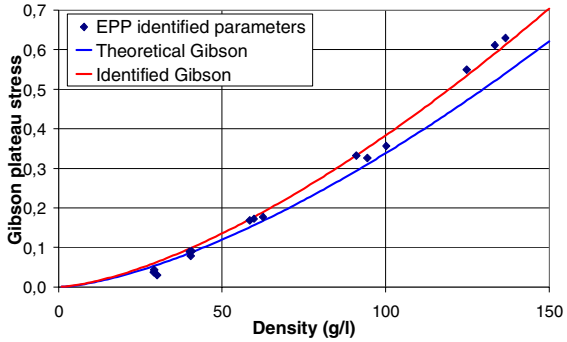

Figure 15. Gibson model for the EPP foams: identified plateau stress parameters, theoretical parameter-density relation and identified relation.

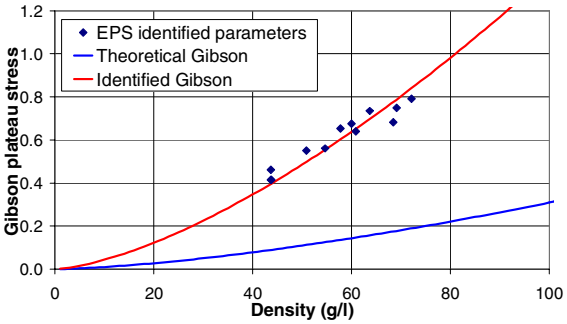

Figure 16. Gibson model for the EPS foams: identified plateau stress parameters, theoretical parameter-density relation and identified relation.

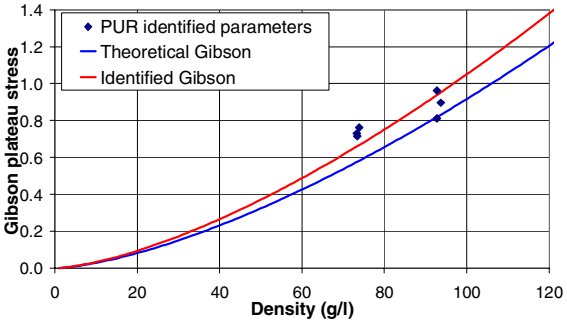

Figure 17. Gibson model for the PUR foams: identified plateau stress parameters, theoretical parameter-density relation and identified relation.

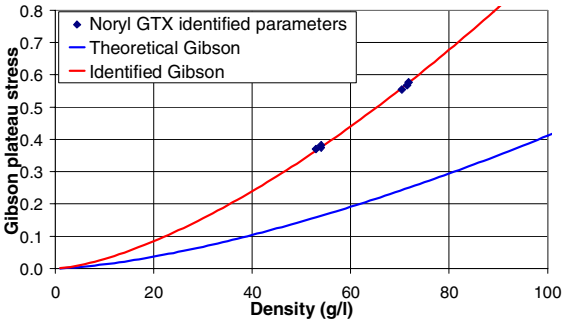

Figure 18. Gibson model for the Noryl GTX foams: identified plateau stress parameters, theoretical parameter-density relation and identified relation

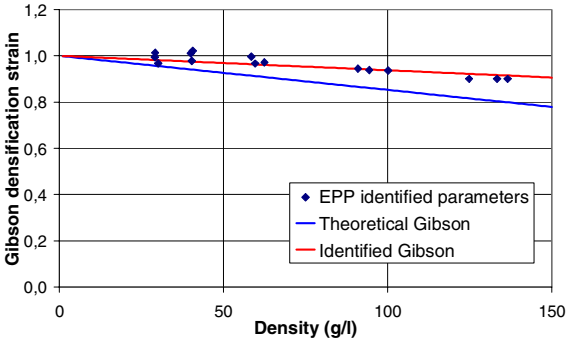

Figure 19. Gibson model for the EPP foams: identified desification strain parameters, theoretical parameter-density relation and identified relation.

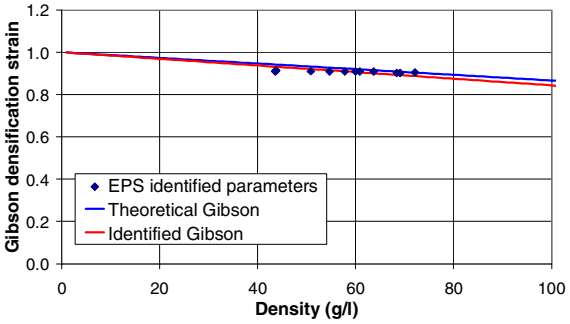

Figure 20. Gibson model for the EPS foams: identified densification strain parameters, theoretical parameter-density relation and identified relation.

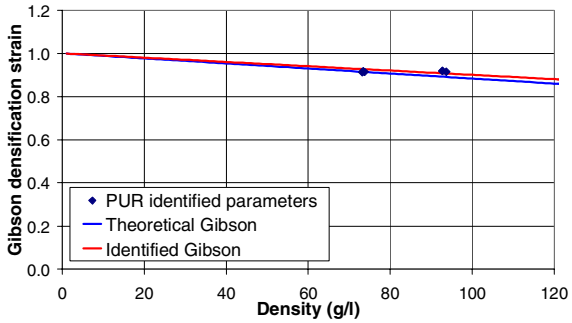

Figure 21. Gibson model for the PUR foams: identified densification strain parameters, theoretical parameter-density relation and identified relation.

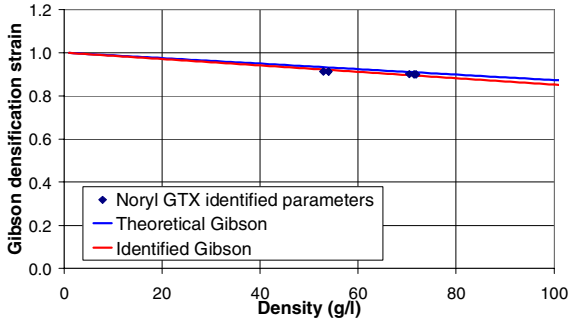

Figure 22. Gibson model for the Noryl GTX foams: identified densification strain parameters, theoretical parameter-density relation and identified relation.

Table 1.
Identified coefficients of the density dependence laws of the Gibson model. The values suggested by Gibson are in brackets.

foam	C_E (Gibson)	C_y (Gibson)	C_D (Gibson)
EPP	1.01e-3 (1.33e-3)	3.83e-4 (3.38e-4)	6.25e-4 (1.47e-3)
EPS	3.44e-3 (2.00e-3)	1.37e-3 (3.09e-4)	1.56e-3 (1.33e-3)
PUR	3.24e-3 (1.11e-3)	1.05e-3 (9.17e-4)	9.96e-4 (1.17e-3)
Noryl GTX	5.04e-3 (1.82e-3)	9.46e-4 (4.11e-4)	1.48e.3 (1.27e-3)

Density Independent Parameters

The parameter D and m are considered density independent and Gibson suggests the values *D=2.3* and *m=1±0.4* for the plastic collapse foams.

In this work a unique value of each parameter has been identified directly from the experimental data of the whole set of tested foams of the same type. The identified values for each kind of foam are shown in Table 2.

Table 2.
Identified density independent parameters.

foam	D	m
EPP	1.01	1.29
EPS	1.34	0.73
PUR	2.73	1.07
Noryl GTX	0.84	0.73

6.2 Modified Gibson Model

As for the original Gibson model the parameters-density laws for the modified Gibson model have been identified and compared with the theoretical Gibson laws. In this case a new parameter is analysed: the slope of the plateau stress. The identified coefficients of the density dependence laws are in Table 3.

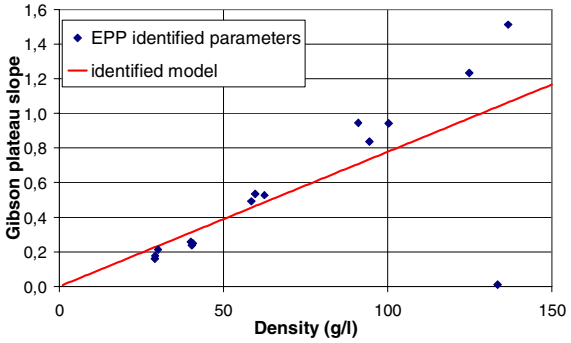

Figure 23. Linear density dependence law of the slope *h* parameter identified for the EPP foams.

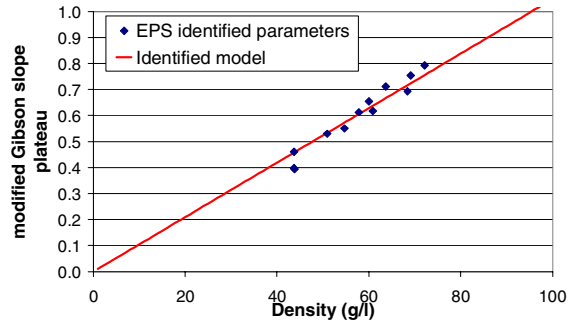

Figure 24. Linear density dependence law of the slope *h* parameter identified for the EPS foams.

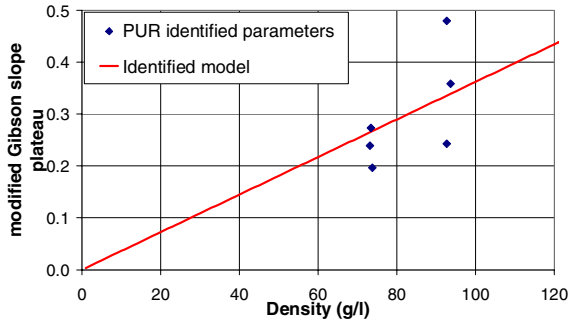

Figure 25. Linear density dependence law of the slope *h* parameter identified for the PUR foams.

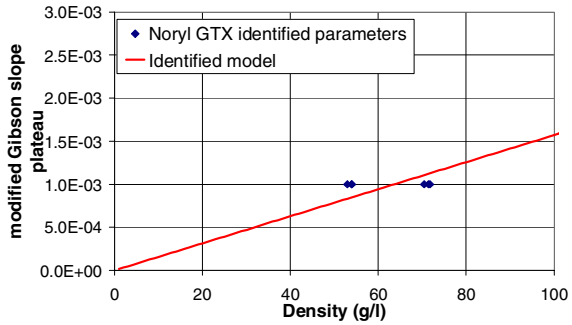

Figure 26. Linear density dependence law of the slope *h* parameter identified for the Noryl GTX foams.

The identified values of this parameter for the tested foams are highly dispersed at higher density values and for certain type of foam. In same cases they are not significant. This could be caused by the fact that the plateau region is limited for higher density foams till to be completely excluded from the model. The identified value for an EPP specimen at 145 g/l is nearly zero: the model in this case shows a shift from the linear region directly to the densification region. The same thing happens for all Noryl GTX foams where the plateau region is completely unused and its slope remains at the initially assigned value: this is confirmed by the identical behaviour of the Gibson model and the modified Gibson model for this type of foam.

Because of this behaviour a density dependence law is difficult to be defined for this parameter and a simple linear law has been identified. The identified curves for each kind of foam are shown in Figures 23-26.

7. MODELS AS A DESIGN TOOL

Test results can be shown in different forms depending on the foam characteristics to be studied and the design purposes. The effects of the foam density have been underlined as the first design parameter to be chosen.

Force-displacement and stress-strain curves, directly derived from the experimental data, show the capability of cellular solids to absorb a high quantity of energy maintaining a nearly constant level of stress in the so called plateau region, but they do not allow directly selecting the foam density suitable to the designed maximum stress and energy amount to be absorbed. The energy versus stress curves are more useful to this aim.

Table 3.
Identified coefficients of the density dependence laws of the modified Gibson model.

foam	C_E	C_y	C_S	C_D
EPP	1.02e-3	3.70e-4	7.80e-3	7.10e-4
EPS	3.51e-3	1.14e-3	1.05e-2	1.20e-3
PUR	3.22e-3	9.46e-4	3.62e-3	8.97e-4
Noryl GTX	5.04e-3	9.46e-4	1.57e-5	1.48e-3

The use of an efficiency coefficient is an even more interesting solution to show the optimal impact loading conditions for defined foam. The efficiency of foam in impact absorption is defined as the ratio of the absorbed energy to the maximum stress value:

$$Efficiency = \frac{W}{\sigma_{max}} \qquad (14)$$

Each foam should be used on the impact energy and maximum stress value defined by its maximum efficiency conditions [5-6].

The proper foam density has to be chosen in order to reach the maximum efficiency on the basis of the defined impact energy to be absorbed and the maximum acceptable stress level. It has to be noted that the foam density with the maximum efficiency for the defined application, corresponds to the foam density which reaches the maximum absorption of energy with the defined maximum level of stress or, likewise, to the foam density which need the minimum stress level to absorb the defined impact energy.

Energy-stress curves, for the EPP foams, and efficiency-stress and efficiency-density curves, for all tested materials, are shown in Figures 27-35. The experimental diagrams that express a given quantity as function of the density result in a set of test points

and not in continuous curves. It is not feasible to examine the density at too many levels.

Modelling can be used to simplify the foam selection. The identified models with its parameters-density laws bring a general model of all possible foams obtained from the same constitutive material and same microstructure. This allows predicting the mechanical behaviour of foam of any density with a minimum set of experimental tests.

Moreover, modelling allows evaluating the energy-stress, energy-density, stress-density, efficiency-stress and efficiency-density curves for any maximum level of stress or absorbed energy. The efficiency-density curves of all tested foams at a defined stress value have been drawn over the experimental data in previous diagrams. These curves clarify the possibility of the models to precisely evaluate the optimal foam density even at the limits of the experimental domain or between two relatively different experimental values of the density.

By means of the identified modified Gibson model and with the help of automated routines, various diagrams have been constructed in order to help foam component design. If the stress limit (acceleration limit) is the main objective of the design, density versus stress curves are to be used. These model-based curves are shown in Figure 36 for the tested materials. These curves bring out the foam density value that allows for the maximum efficiency while maintaining a defined maximum stress. These diagrams lead to the choice of the optimal density, but do not show the energy involved: the dimensions of the foam have to be chosen with an energy diagram.

A diagram which incorporates all the design parameters must contain more curves. For example, several specific absorbed energy versus density curves for a wide range of maximum stress values combine all information about a specific kind of foam. This kind of diagrams have been constructed on the basis of the modified Gibson model and are shown in Figures 37-40 for each analysed type of foam.

The modified version of the Gibson model compared to the original Gibson model has demonstrated to be more suitable to be used in numerical procedures for the construction of proposed design diagrams. It has the advantage to be strictly increasing and consequently to have a unique strain value for a defined stress. On the contrary the original Gibson model has an undefined value of strain corresponding to the plateau stress and it can cause problem in numerical procedures definition.

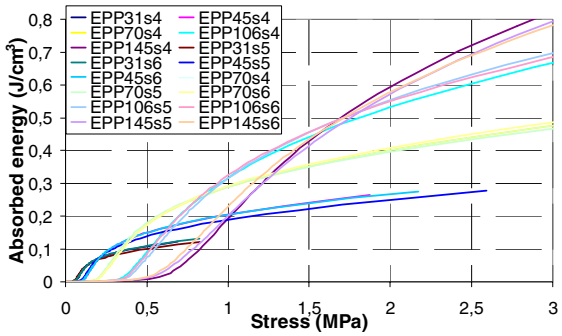

Figure 27. Specific energy-stress experimental curves for the EPP foams.

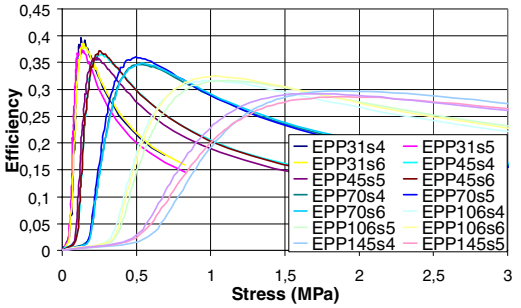

Figure 28. Experimental efficiency-stress curves for EPP foams.

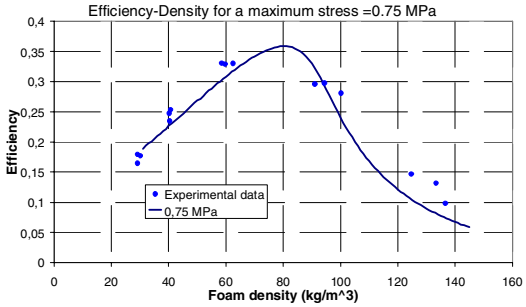

Figure 29. Experimental efficiency points at a defined stress of 0.75 MPa and model curve for EPP foams.

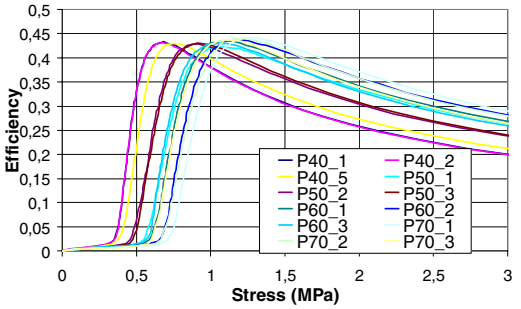

Figure 30. Experimental efficiency-stress curves for EPS foams.

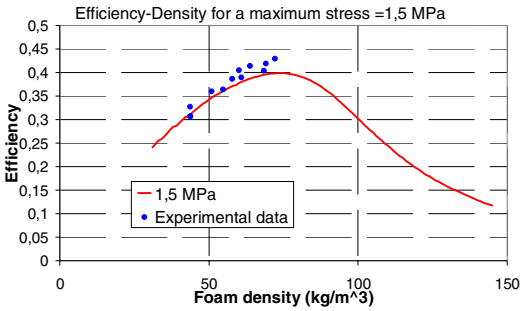

Figure 31. Experimental efficiency points at a defined stress of 1.5 MPa and model curve for EPS foams.

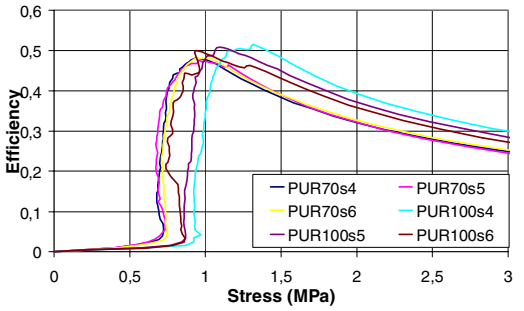

Figure 32. Experimental efficiency-stress curves for PUR foams.

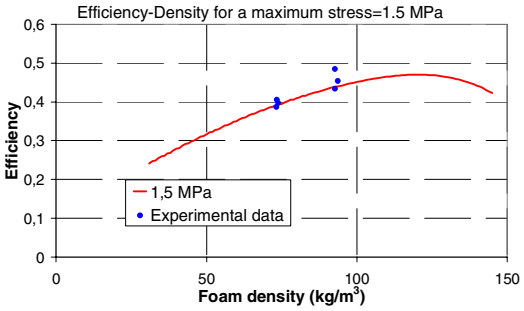

Figure 33. Experimental efficiency points at a defined stress of 1.5 MPa and model curve for PUR foams.

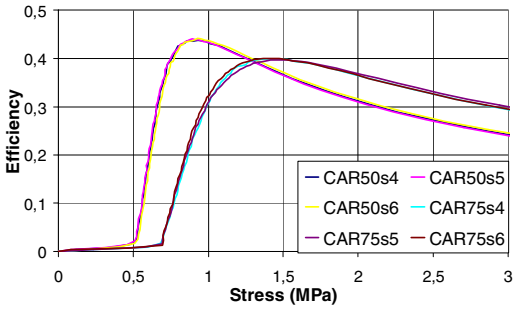

Figure 34. Experimental efficiency-stress curves for Noryl GTX foams.

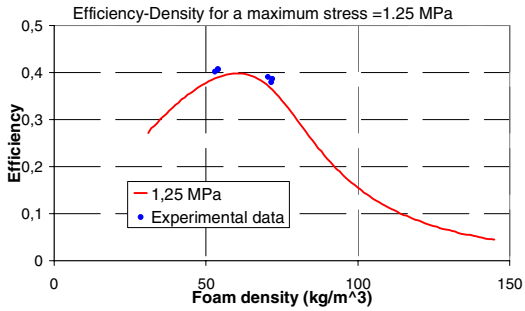

Figure 35. Experimental efficiency points at a defined stress of 1.25 MPa and model curve for Noryl GTX foams.

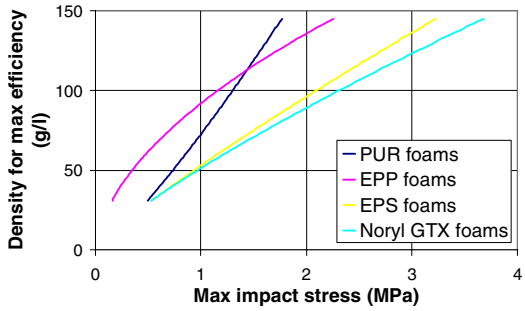

Figure 36. Modeled optimal density versus maximum stress curves for all tested foams.

8. CONCLUSIONS

All analysed and identified cellular solid models fit well the experimental curves of the four kinds of foam tested. The Gibson Model and the modified version of this model show a better fitting capability compared to the Rusch model and the modified Rusch model. The identification, by means of optimisation procedures, has been slower because of the three different formulations for each stress-strain region.

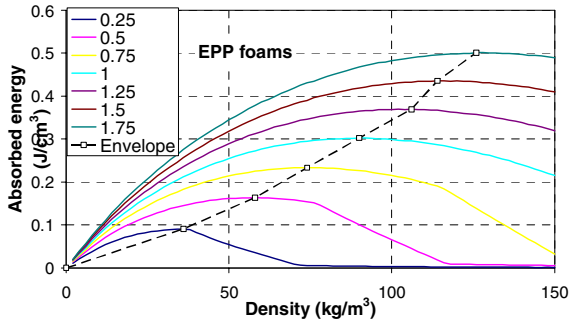

Figure 37. Modeled (modified Gibson) specific absorbed energy versus density curves for different stress level and envelope of their maximum for EPP foams.

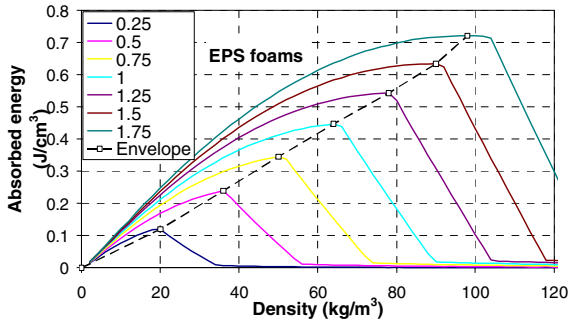

Figure 38. Modeled (modified Gibson) specific absorbed energy versus density curves for different stress level and envelope of their maximum for EPS foams.

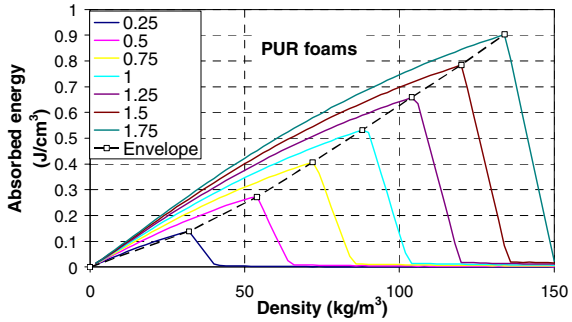

Figure 39. Modeled (modified Gibson) specific absorbed energy versus density curves for different stress level and envelope of their maximum for PUR foams.

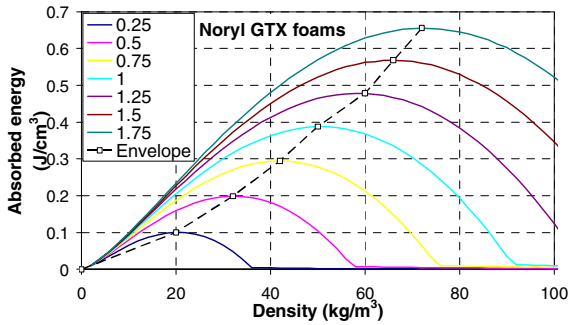

Figure 40. Modeled (modified Gibson) specific absorbed energy versus density curves for different stress level and envelope of their maximum for Noryl GTX foams.

The micro-mechanical density dependence laws of the Gibson model have been identified by means of the experimentally obtained parameters for different densities of the same type of foam. These laws have been compared to the simplified relations suggested by Gibson and in some cases have shown to be significantly different.

The density dependence laws have been identified also for the modified Gibson model. For the newly introduced parameter, the slope of the plateau region, a linear density dependence law has been considered.

The density dependence laws combined with the foam models permit complete modelling of a certain type of foam on a wide range of density, by testing very few values of density. This is useful for an effective choice of the proper foam density for a specific application. Energy diagrams, efficiency curves (shown in [5]) and any other kind of diagrams that describe the effect of density could be obtained by means of the modified Gibson model and few experimental tests. This kind of modelling has shown to be an efficient tool in optimal design of impact absorbers for passive safety of vehicles.

REFERENCES

[1] L. J. Gibson and M. F. Ashby. 1997. "Cellular Solid Structure and Properties". Cambridge University Press.

[2] K.C. Rush. 1969. "Load-Compression Behavior of Flexible Foams". Journal of Applied Polymer Science, 13, 2297-2311.

[3] K.C. Rush. 1970. "Energy-Absorbing Characteristics of Foamed Polymers". Journal of Applied Polymer Science, 14, 1133-1147.

[4] K.C. Rush. 1970. "Load-Compression Behaviour of Brittle Foams". Journal of Applied Polymer Science, 14, 1263-1273.

[5] M. Avalle, G. Belingardi and R. Montanini. 2001. "Characterization of polymeric structural foams under compressive impact loading by means of energy-absorption diagram". International Journal of Impact Engineering, 25, 455-472.

[6] M. Avalle, G. Belingardi and A. Ibba. 2004. "Experimental Testing of Cellular Solids and Model Parameters Identification". 12th International Conference on Experimental Mechanics.